



IGAM/UniGraz Technical Report for ASA No. 1/2004

ASA study:

CHAMPCLIM – Radio Occultation Data Analysis Advancement and Climate Change Monitoring based on the CHAMP/GPS Experiment

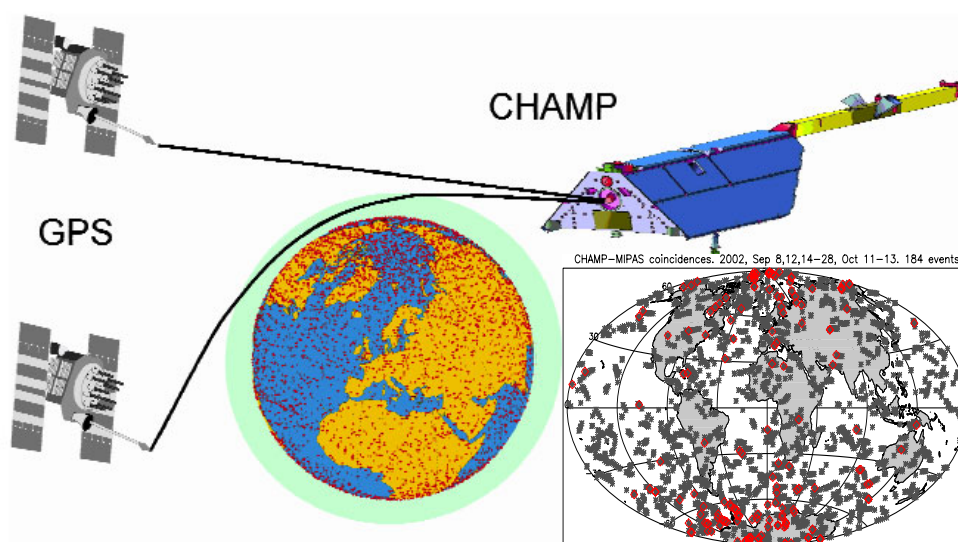
[Contract No: ASAP-CO-004/03 – July 2003]

VALIDATION REPORT

[WP2: VALIDATE]

Radio Occultation Data and Algorithms Validation Based on CHAMP/GPS Data

A. Gobiet, A.K. Steiner, C. Retscher, U. Foelsche, and G. Kirchengast
Institute for Geophysics, Astrophysics, and Meteorology (IGAM),
University of Graz, Graz, Austria



Final Version – April 2004

(intentionally left blank, back page if double-sided print)

Table of Contents

1 INTRODUCTION.....	1
2 IGAM RO RETRIEVAL ALGORITHM OVERVIEW	2
2.1 General RO Retrieval	2
2.2 RO Retrieval at High Altitudes.....	3
3 VALIDATION SETUP	5
3.1 Description of Data.....	5
3.1.1 Simulated Data.....	5
3.1.2 CHAMP/GPS Retrieval Validation and Intercomparison Data	6
3.1.3 ECMWF Data	9
3.1.4 ENVISAT/MIPAS and ENVISAT/GOMOS Data	9
3.2 Validation Methodology	13
4 VALIDATION RESULTS.....	15
4.1 Simulation Study	15
4.2 IGAM – GFZ Retrieval Intercomparison	16
4.3 Validation with Independent Data Sources	19
4.3.1 ECMWF-NWP analyses	20
4.3.2 MIPAS	26
4.3.3 GOMOS HRTP	28
4.3.4 GOMOS/IGAM	30
5 CONCLUSIONS AND OUTLOOK	31
Acknowledgments.....	32
References	33
Appendix A: CHAMP – ECMWF Error Statistics, Compiled	37
Appendix B: CHAMP – ECMWF Tropopause Temperature Differences, Examples ..	41

(intentionally left blank, back page if double-sided print)

1 Introduction

Observing and detecting changes and variability in the global climate is one of the most important challenges in atmospheric sciences over the coming decades, since there exists concern and evidence that the Earth's climate is increasingly influenced by human activities (e.g., IPCC, 2001). Global warming and climate change in general is not only a scientific but also a political topic, which makes it especially important to establish reliable and stable long-term records of atmospheric temperature. The Global Navigation Satellite System (GNSS) Radio Occultation (RO) technique is an active limb sounding method using GNSS radio signals to probe the Earth's atmosphere (see Fig. 1 for a sketch of the measurement geometry). Its high vertical resolution (0.5 to 1.5 km), high accuracy (the temperature error is less than 1 K in the upper troposphere and lower stratosphere), its long-term stability (less than 0.1 K per decade is expected), all-weather capability, and global coverage suggests the RO technique as a promising tool for long-term monitoring of the Earth's climate (Kirchengast et al., 2000; Anthes et al., 2000; Steiner et al., 2001).

The successful “proof-of-concept” experiment GPS/MET (1995–1997) demonstrated these unique characteristics (Ware et al., 1996; Kursinski et al., 1996; Rocken et al., 1997; Steiner et al., 1999). The German/U.S. research satellite CHAMP, which was launched on July 15, 2000, and continuously provides more than 200 globally distributed occultation events per day (of which ~170 atmospheric profiles can be retrieved, Wickert et al., 2004b), is the first opportunity for realizing global RO based climatologies.

The prime objective of the CHAMPCLIM project is to help ensure that the CHAMP/GPS RO data are exploited in the best possible manner for climate monitoring by addressing three areas: 1) CHAMP RO data and algorithms validation, 2) CHAMP/GPS-based RO data processing advancements in order to optimize the climate utility of the data, and 3) CHAMP/GPS-based monitoring of climate variability and change, respectively. This report is a documentation of the validation work carried out during the first year of the project (area 1, work package 2 of the CHAMPCLIM project plan). It is tightly connected to area 2 (RO data processing advancements) and will briefly address some data processing topics as well.

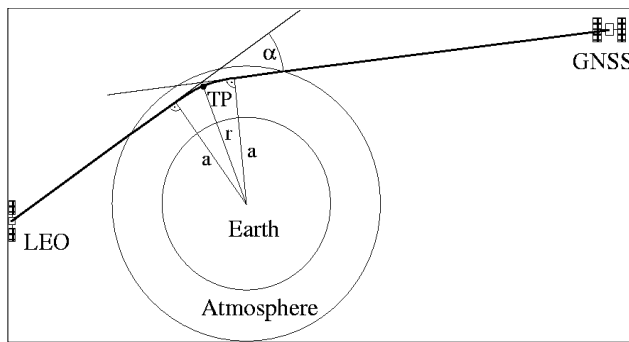
Sect. 2 of this report gives a brief overview of the RO retrieval technique and some advancements achieved over the last year (more details about RO retrieval advancements will be given in the “Advancement Report” documenting area 2 of the project). In Sect. 3 we describe the reference data samples and the methods used for the validation. In Sect. 4 we present a simulation study for validating RO retrieval algorithms and an intercomparison study between the operational CHAMP-RO retrieval algorithms of GeoForschungsZentrum Potsdam (GFZ) and algorithms developed at IGAM. Furthermore, we show results on the comparison with different independent data sources. Finally, in Sect. 5, conclusions are drawn and a brief outlook on our future work is presented.

2 IGAM RO Retrieval Algorithm Overview

2.1 General RO Retrieval

The basic idea of RO retrieval is based on the geometric optics assumption, i.e., the radio signals emitted by GNSS satellites are treated as rays. This simplification is valid from the mid-troposphere upwards, below some 5 km, however, wave-optics methods can significantly improve the retrieval in order to cope with complex signal structures in the presence of strong refractivity gradients (e.g., Hocke et al., 1999; Gorbunov, 2002; Sokolovskiy, 2003; Beyerle et al., 2003; Jensen et al., 2003). Since this study mainly focuses on the retrieval performance in the stratosphere and on the influence of background information on the retrieval in high altitudes, only geometric optics retrieval was performed and will be briefly outlined in the following paragraphs.

The primary observables of RO measurements are phase delays of GNSS signals (GPS: L1, $f_1 = 1575.42$ MHz; L2, $f_2 = 1227.60$ MHz) resulting from the deceleration of the electromagnetic wave's phase velocity by the atmosphere. Doppler shifts and total bending angles α as a function of the ray's impact parameters a are deduced from the phase delays (e.g., Kursinski et al., 1997). The refractive index n can then be derived via an inverse Abel transform (Eq. 2.1, Fjeldbo et al., 1971),



$$n(a) = \exp \left[\frac{1}{\pi} \int_a^{\infty} \frac{\alpha(a')}{\sqrt{a'^2 - a^2}} da' \right], \quad (2.1)$$

Fig. 2.1: Radio occultation geometry (after Foelsche, 1999).

from which the refractivity as a function of height $N(z)$ is obtained via $N(a) = 10^6(n(a) - 1)$ and $z(a) = a/n(a) - R_C$. R_C is the radius of curvature of the earth's ellipsoid at the occultation location (\sim Earth's radius), a is the ray's impact parameter. Other atmospheric parameters, such as pressure, geopotential height, temperature, and humidity, are derived from refractivity using the refractivity equation (Eq. 2.2), the hydrostatic equation, and the equation of state (ideal gas law). Refractivity is related to total atmospheric pressure p , temperature, T , and the partial pressure of water vapor, p_w , via

$$N = k_1 \frac{p}{T} + k_2 \frac{p_w}{T^2}. \quad (2.2)$$

k_1 and k_2 are constants ($k_1 = 77.60 \pm 0.05 \text{ K hPa}^{-1}$, $k_2 = 3.739 \cdot 10^5 \pm 0.012$, Bevis et al., 1994). Eq. (2.3) describes the calculation of dry pressure $p_d(z)$ which is equal to the atmospheric pressure if humidity can be neglected ($p_w = 0$), i.e., everywhere above the lower to middle troposphere.

$$p_d(z) = \frac{M_d}{k_1 R} \int_z^{\infty} g(z') N(z') dz' \quad (2.3)$$

R is the universal gas constant ($8.314 \cdot 10^3 \text{ J K}^{-1} \text{ kg}^{-1}$), M_d is the molecular mass of dry air ($28.966 \text{ kg kmol}^{-1}$), and $g(r)$ is the gravitational acceleration. The dry temperature T_d can then be derived from Eq. (2.2) by neglecting the effect of water vapor which is valid in the mid- to upper troposphere and stratosphere. Below $\sim 6 \text{ km}$, a priori information about either the temperature or the humidity is necessary to derive one of these parameters. Since this report focuses on the retrieval performance at high altitudes and the problems arising there (see Sect. 2.2), we only validate refractivity (which is insensitive to the above mentioned ambiguity) and dry temperature.

2.2 RO Retrieval at High Altitudes

Ionospheric effects dominate the bending angles at heights above $\sim 45 \text{ km}$ (Hocke, 1997). Since the ionosphere, as a dispersive medium, causes different L1 and L2 phase delays, these effects can be removed to first order by linear combination of the two signals. In recent applications the method of linear correction of bending angles (Eq. 2.4, Vorob'ev and Krasil'nikova, 1994) has been applied most successfully:

$$\alpha_{LC}(a) = \frac{f_1^2 \alpha_1(a) - f_2^2 \alpha_2(a)}{f_1^2 - f_2^2}, \quad (2.4)$$

where α_{LC} is the ionosphere-corrected bending angle, α_1 , and α_2 are the uncorrected bending angles of the L1 and L2 rays, respectively.

Even after ionospheric correction, retrieval results at heights above $20 - 30 \text{ km}$ are sensitive to residual ionospheric noise (higher order terms, that can not be corrected by Eq. 2.4) and other error sources such as orbit uncertainties, local multipath errors, receiver noise, and residual clock errors. Since its upper integration limit ranges to infinity, the inverse Abel transform (Eq. 2.1) needs, in practice, some kind of high altitude initialization to avoid downward propagation of errors via the inverse Abel transform and subsequently via the hydrostatic integration (Eq. 2.3). To keep these errors minimal, the concept of statistical optimization was introduced into the field of RO retrieval (Sokolovskiy and Hunt, 1996). It derives the best linear unbiased estimator (BLUE, Eq. 2.5), α_{opt} , from an observed (α_o) and a background (α_b) bending angle profile under the assumption of unbiased Gaussian errors. \mathbf{O} and \mathbf{B} are the observation and background error covariance matrices, respectively.

$$\alpha_{opt} = \alpha_b + \mathbf{B}(\mathbf{B} + \mathbf{O})^{-1}(\alpha_o - \alpha_b) \quad (2.5)$$

α_{opt} is a fused bending angle profile dominated by background information in the upper part and by the observation in the lower part. Though most recent retrieval schemes initialize

RO Data and Algorithms Validation Based on CHAMP/GPS Data

CHAMPCLIM – Radio Occultation Data Analysis and Climate Monitoring based on CHAMP/GPS

the hydrostatic integral with a pressure value derived from a temperature guess at 40 – 50 km, this is not necessary if the refractivity profile derived from Eq. (2.1) reaches high enough (~ 120 km). The IGAM retrieval schemes integrate background information only at one point of the retrieval (at bending angle level), so that the results have well defined error characteristics. We implemented statistical optimization in two different ways, both relying on Eq. (2.5), but using different sources of background information and different ways of pre-processing of this information: IGAM/MSIS uses bending angle profiles extracted from the MSISE-90 climatology (Hedin, 1991) and applies best-fit-profile library search and bias correction procedures (Gobiet and Kirchengast, 2004) in order to diminish known biases in the climatology (Randel et al., 2002). IGAM/ECMWF uses bending angle profiles derived from ECMWF operational analyses. More details about the IGAM retrieval schemes can be found in Tab. 1. Both schemes are geometric optics dry air retrievals.

Table 2.1: Overview of the IGAM CHAMP-RO retrieval schemes (EGOPS/CCR Version 2, March 2004).

	IGAM/MSIS	IGAM/ECMWF
Outlier Rejection and Smoothing	“ 3σ ” outlier rejection on phase delays and smoothing using regularization.	Like IGAM/MSIS
Ionospheric Correction	Linear combination of bending angles (Vorob’ev and Krasil’nikova, 1994). Correction is applied to low-pass filtered bending angles (1 km sliding average), L1 high-pass contribution is added after correction (Hocke et al., 2003). L2 bending angles < 15 km derived via L1-L2 extrapolation.	Like IGAM/MSIS
Bending Angle Initialization	Statistical optimization of bending angles 30 – 120 km. Vertical correlated background (corr. length $L = 6$ km) and observation ($L = 1$ km) errors. Obs. error estimated from obs. profile >60 km. Background error: 15 %. Backg. information: MSISE-90 best fit-profile, bias corrected (Gobiet and Kirchengast, 2004).	Like IGAM/MSIS, but co-located bending angle profile derived from ECMWF operational analysis (above ~60 km: MSISE-90) as backg. information. No further pre-processing.
Hydrostat. Integral Init.	At 120 km: pressure = $p(\text{MSISE-90})$.	Like IGAM/MSIS
Quality Control	Refractivity 5 – 35 km: $\Delta N/N < 10 \%$; Temperature 8 – 25 km: $\Delta T < 25$ K. Reference: ECMWF analysis.	Like IGAM/MSIS

3 Validation Setup

This section gives a description of the data and the methodologies used for the retrieval validation. The validation of the IGAM RO retrieval schemes was performed in three stages, the results of each of them is presented in one subsection of Sect. 4: In Sect. 4.1 simulated RO observations are used to rate the IGAM retrieval performance (see Sect. 3.1.1 for the description of the simulated data set). In Sect. 4.2, the IGAM retrieval is applied to CHAMP phase delay data (provided by the CHAMP Information System and Data Center (ISDC)) and compared to operational retrieval results from GFZ (see Sect. 3.1.2 for the description of the involved datasets). In Sect. 4.3, the IGAM retrieval results are compared to independent data, namely coinciding profiles derived from operational analysis fields from the European Centre for Medium-Range Weather Forecasts (ECMWF, Sects. 3.1.3 and 4.3.1) and coinciding temperature profiles from the MIPAS and GOMOS instruments onboard ENVISAT (see Sects. 3.1.4 and 4.3.2 – 4.3.4).

3.1 Description of Data

3.1.1 Simulated Data

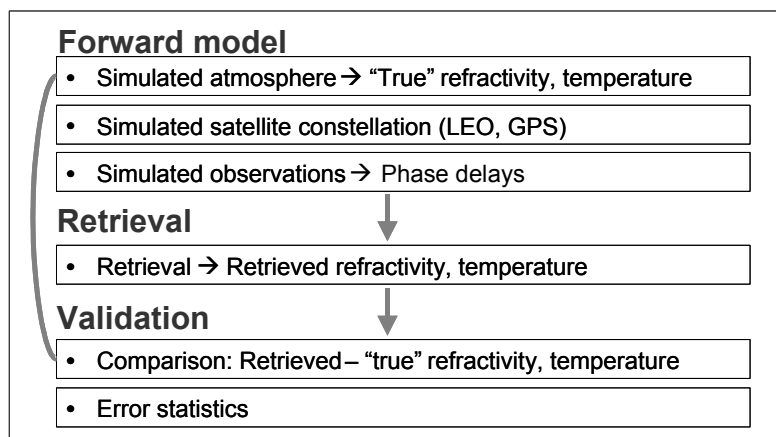


Figure 3.1: Schematic sketch of the end-to-end simulation study setup.

For a first validation of the performance of remote sensing systems end-to-end simulation studies are ideal tools, since one has a perfect knowledge of the “truth” and easily can add or remove simulated error sources. In preparation for the application of the IGAM retrieval schemes on real CHAMP data, we performed such a simulation study. It was realized by means of a modified version of the EGOPS software tool (End-to-end GNSS Occultation Performance Simulator, Kirchengast et al., 2001). It involved the simulation of a constellation of six satellites in low earth orbit (LEO), each equipped with a receiver for setting and rising occultations, modeling of the neutral atmosphere with the ECHAM4 General Circulation Model (Roeckner et al., 1999), and modeling of the ionosphere via the NeUoG model (Leitinger and Kirchengast, 1997). The LEO constellation geometry and the two models were used to create simulated RO observations (“forward model”) that, in turn, were input for the

retrieval algorithm to derive atmospheric profiles (“inversion”). See Fig. 3.1 for a schematic sketch of the end-to-end simulation setup.

The sample of simulated RO observations consists of ~ 1000 occultation events (selected from a sample of about 13 000 events) that characterize the summer season 1997 (June, July, and August) and are evenly distributed in time and space in a latitudinal slice of the globe. It is partitioned into 17 equal area latitude bins of 10° width (equatorial bin: 10° lat x 15° lon), each containing 50–60 occultation events (Fig. 3.2, Foelsche et al., 2003).

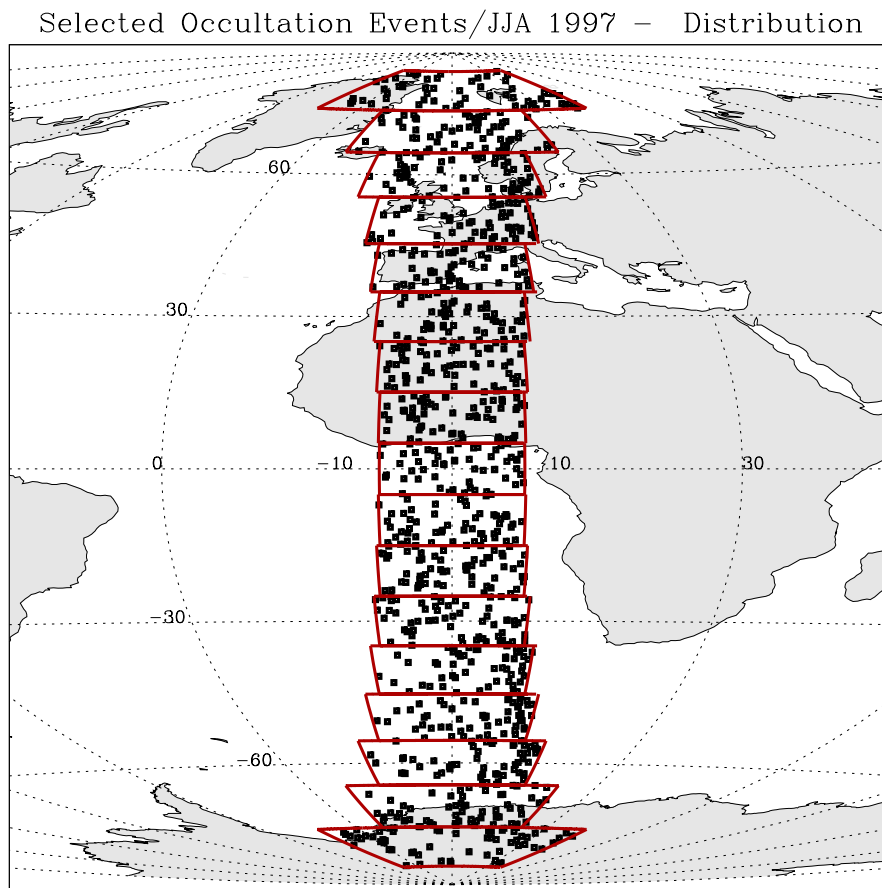


Figure 3.2: Distribution of 979 occultation events comprising the validation ensemble in the end-to-end simulation study. After: Foelsche et al. (2003).

3.1.2 CHAMP/GPS Retrieval Validation and Intercomparison Data

For validating atmospheric profiles retrieved from CHAMP measurements, three different datasets were used according to the availability of correlative data. Starting from CHAMP-phase delays provided by GFZ Potsdam (GFZ level 2 data, version 2), we applied the IGAM/MSIS and the IGAM/ECMWF retrieval schemes (EGOPS/CCR version 2) as described in Sect. 2 in order to derive atmospheric profiles such as refractivity and temperature.

These profiles were analyzed and validated against different data sources as described in this and the two following subsections. In addition to the analysis of the global ensemble of measurements, the data sets were separated into three latitude bands, low (-30° to $+30^\circ$), middle ($\pm 30^\circ$ to $\pm 60^\circ$), and high ($\pm 60^\circ$ to $\pm 90^\circ$) in order to account for the different mean state of the atmosphere and ionosphere at different latitudes. This is especially important in

order to judge the success of the ionospheric correction which faces a more complicated situation at low latitudes (equatorial anomaly, spherical asymmetry, small-scale structures causing scintillations in the RO signal) than at mid- and high latitudes. Additionally, the dry and stable conditions in the high-latitude troposphere represent much easier conditions for the RO retrieval than the moist and highly variable equatorial troposphere.

Based on the latitudinal classification, the CHAMP occultation events are roughly equally distributed. However, if one refers to commensurate areas, the measurement density near the poles is much higher than at low latitudes. This is due to the high inclination ($i = 87^\circ$) of the CHAMP orbit and results in an increased observational coverage at high latitudes (see Figs. 3.3 – 3.5).

Basic characteristics of RO-derived atmospheric profiles that have to be regarded when comparing them to other data sources are the low horizontal and high vertical resolution, (~ 250 km and ~ 1 km, respectively, depending on the tangent height of the radio path and the state of the atmosphere, e.g., Kursinski et al., 1997) and the fact that RO profiles are generally not vertical with the average zenith angle of the tangent point trajectory near the Earth's surface being about 85° .

CHAMP Data for the IGAM – GFZ Retrieval Intercomparison

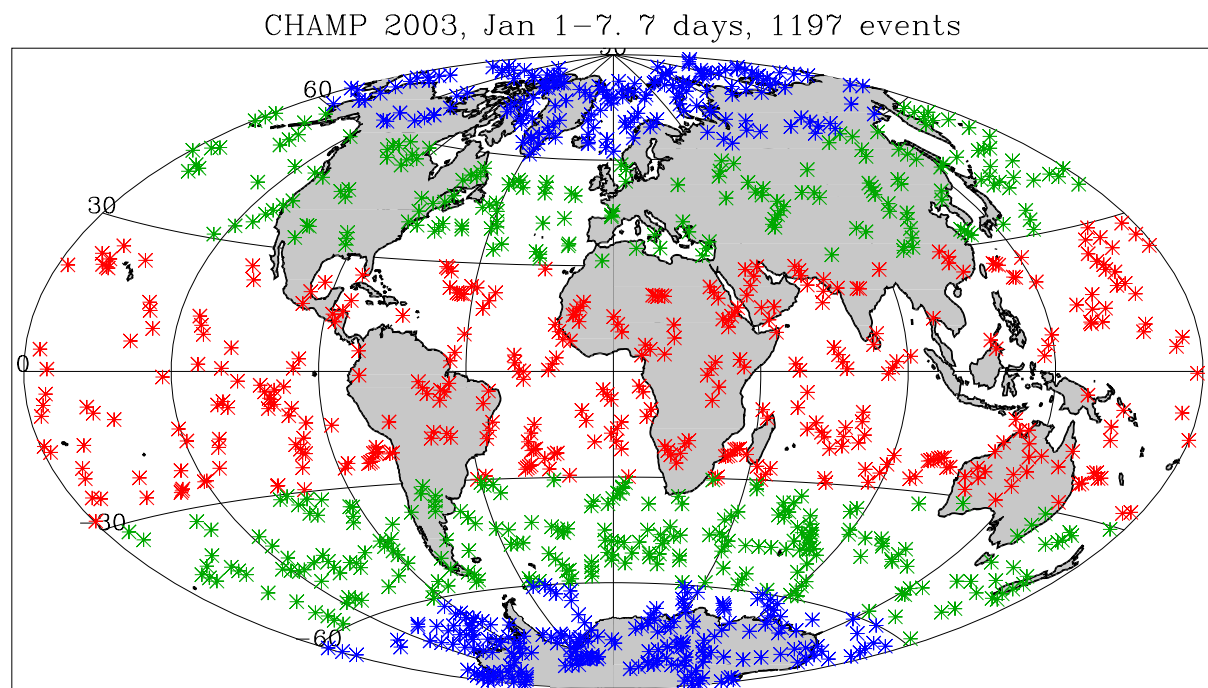


Figure 3.3: CHAMP data retrieved by IGAM for retrieval intercomparison with GFZ: Distribution of 1197 atmospheric profiles (Jan 1 – 7, 2003). The whole sample is separated into three latitude bands: low (-30° to $+30^\circ$, 377 events), middle ($\pm 30^\circ$ to $\pm 60^\circ$, 436 events), and high ($\pm 60^\circ$ to $\pm 90^\circ$, 384 events).

For the intercomparison of GFZ- and IGAM-derived atmospheric profiles from CHAMP phase delay data, a 7-day period (January 1 – 7, 2003) was selected. The IGAM/MSIS (see Fig. 3.3) and IGAM/ECMWF retrieval schemes applied to the GFZ level 2 data of this period yielded 1197 and 1187 atmospheric profiles for this period, respectively, which corresponds to about 170 profiles per day on average. These profiles were compared to the operational GFZ atmospheric profiles (level 3, retrieval version 4).

The operational GFZ retrieval yields 1250 atmospheric profiles for the validation period. Due to different data treatment and different quality control schemes at IGAM and GFZ, the IGAM-retrieved profiles do not simply form a sub-set of the GFZ-results, but also contain events that are not available in the GFZ-set. As a result, only the intersection of these sets, 1136 events for the IGAM/MSIS retrieval, and 1130 events for the IGAM/ECMWF retrieval, were available for the comparison study presented in Sect. 4.2 of this report.

CHAMP Data for Comparison with ECMWF Analyses

For the comparison of IGAM retrieval results with ECMWF analyses (Sect. 4.3.1) the same CHAMP data sample as described in the previous section was used (Jan 1 – 7, 2003). Additionally, since there were no restrictions in the availability of ECMWF-data, all IGAM-retrieved CHAMP profiles described in this report were compared to ECMWF analyses and are available for the interested reader in Appendix A.

CHAMP Data for Comparison with MIPAS/GOMOS Temperature Profiles

The study periods for the CHAMP – MIPAS and CHAMP – GOMOS comparisons were restricted by the availability of data from those two ENVISAT instruments (see Sect. 3.1.4 for a description of the ENVISAT datasets). For the MIPAS-study, a 20-day ensemble of CHAMP data from September and October 2002 (Sep 8, Sep 12, Sep 14 – 28, Oct 11 – 13) was used, which corresponds to the MIPAS data availability in this period. The total ensemble consists of 3161 (IGAM/MSIS-retrieval) or 3160 CHAMP occultation events (IGAM/ECMWF-retrieval, see Fig. 3.4), respectively, which corresponds to ~ 160 events per day on average.

CHAMP 2002, Sep 8,12,14–28, Oct 11–13. 20 days, 3160 events.

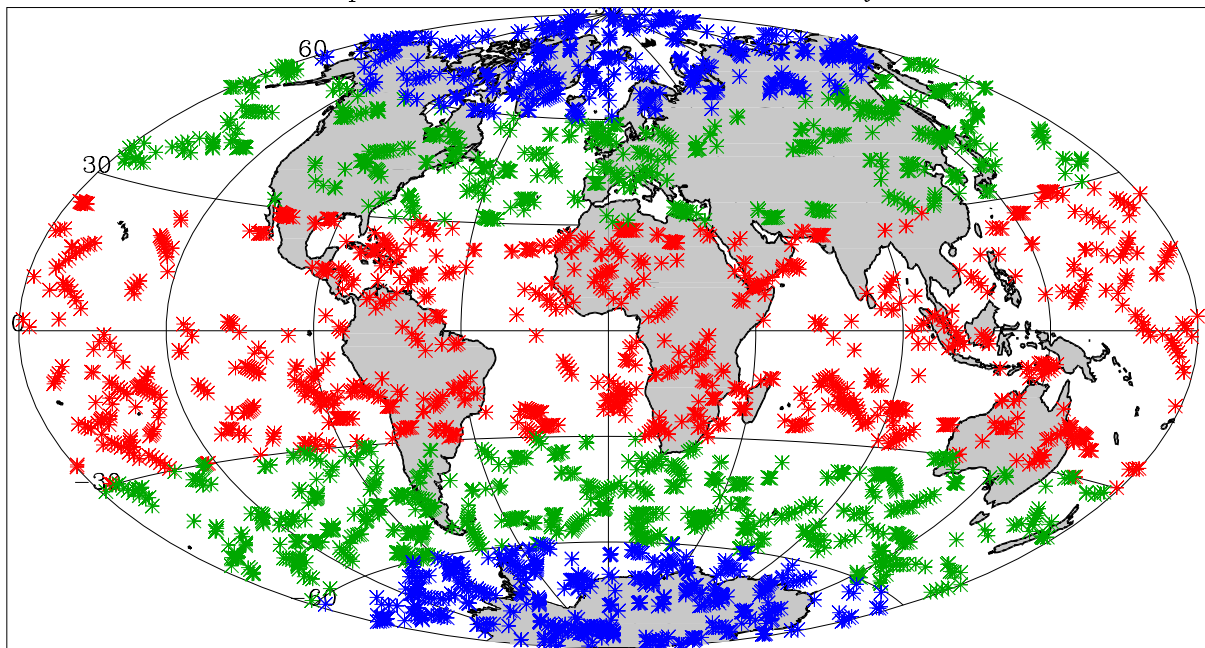


Figure 3.4: CHAMP data retrieved by IGAM for comparison with MIPAS: Distribution of 3160 temperature profiles (Sep 8, 12, 14 – 28, Oct 11 – 13, 2002). The whole sample is separated into three latitude bands: low (-30° to $+30^\circ$, 984 events), middle ($\pm 30^\circ$ to $\pm 60^\circ$, 1222 events), and high ($\pm 60^\circ$ to $\pm 90^\circ$, 954 events).

For the GOMOS-study, a 11-day subset of the ensemble shown in Fig. 3.4 was used (Sep 20 – 27, Oct 11 – 13) corresponding to the GOMOS data availability. The ensemble consists of

1689 (IGAM/MSIS-retrieval) or 1798 CHAMP occultation events (IGAM/ECMWF-retrieval, see Fig. 3.5), respectively which corresponds to ~ 160 events per day on average.

CHAMP 2002, Sep 20–27, Oct 11–13. 11 days, 1798 events

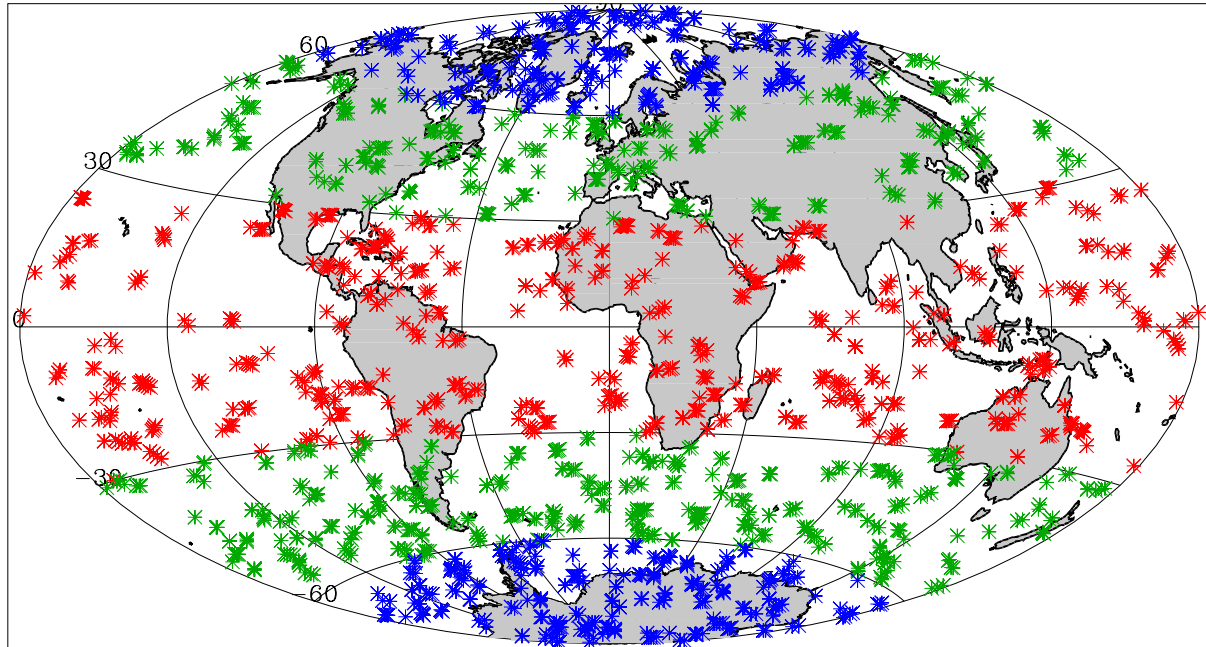


Figure 3.5: CHAMP data retrieved by IGAM for comparison with GOMOS: Distribution of 1798 temperature profiles (Sep 20 – 28, Oct 11 – 13, 2002). The whole sample is separated into three latitude bands: low (-30° to $+30^\circ$, 573 events), middle ($\pm 30^\circ$ to $\pm 60^\circ$, 684 events), and high ($\pm 60^\circ$ to $\pm 90^\circ$, 541 events).

3.1.3 ECMWF Data

As reference data for the comparison of IGAM retrieved CHAMP profiles, co-located vertical temperature and refractivity profiles (assuming fixed mean tangent point latitude and longitude of the CHAMP occultation event) were calculated from the nearest analysis time layer of 6-hourly operational ECMWF analyses, i.e., the time delay between the CHAMP- and the ECMWF-profile is less than 3 hours in any case. The analysis fields were retrieved from ECMWF on a Gaussian grid corresponding to the T42L60 spectral resolution, i.e., on a grid containing 128×64 horizontal grid cells and 60 altitude layers. The horizontal ECMWF-resolution (~ 300 km) roughly corresponds to the horizontal resolution of RO atmospheric profiles. The vertical ECMWF-resolution of 60 levels up to 0.1 hPa, however, is coarser than the RO resolution which has to be regarded in the interpretation of the results.

3.1.4 ENVISAT/MIPAS and ENVISAT/GOMOS Data

In March 2002, the European Space Agency (ESA) launched ENVISAT, a polar-orbiting Earth observation satellite which provides measurements of the atmosphere, ocean, land, and ice. It was put into a sun-synchronous orbit of 98.5° inclination which results in a global coverage and higher observational density at the poles than at the equator. The platform carries ten instruments, amongst those GOMOS, MIPAS and SCIAMACHY are dedicated to the observation of the Earth's atmosphere. The main objective of these instruments is to monitor the chemical composition of the atmosphere but they are also capable of measuring fundamental physical parameters like density and temperature.

Temperature profiles from MIPAS and GOMOS are utilized for comparison with CHAMP profiles in this report. For this purpose, we defined a CHAMP and ENVISAT profile to be coinciding and thus comparable if they are less than 300 km and 3 hours apart from each other using the simplification of fixed mean latitudes and longitudes of the observed profiles.

MIPAS

The Michelson Interferometer for Passive Atmospheric Sounding (MIPAS) is a Fourier transform spectrometer for the measurement of high-resolution gaseous emission spectra at the Earth's limb. Thermal emissions in the infrared are very sensitive to temperature changes and MIPAS is therefore able to measure precise temperature profiles. The MIPAS temperatures used for this study were produced by the Institut für Meteorologie und Klimaforschung (IMK) in Karlsruhe (IMK product version V1.0). Details on the MIPAS retrieval can be found in v. Clarmann et al. (2003a) and v. Clarmann et al. (2003b). ECMWF analyses are used as an initial guess in the iterative MIPAS retrieval process, but not as background constraint as in the IGAM/ECMWF CHAMP retrieval. MIPAS temperatures can therefore be regarded as largely independent from ECMWF data. It is dedicated to distribute atmospheric profiles from 6–70 km altitude with a vertical resolution of 3 km and a horizontal resolution between 300 and 500 km along track. Due to the sensitivity of the measurement principle to clouds, the number of available measurements per day varies from several tens to low hundreds (Wang et al., 2004).

ENVISAT/MIPAS 2002, Sep 8,12,14–28, Oct 11–13. 20 days, 6561 events.

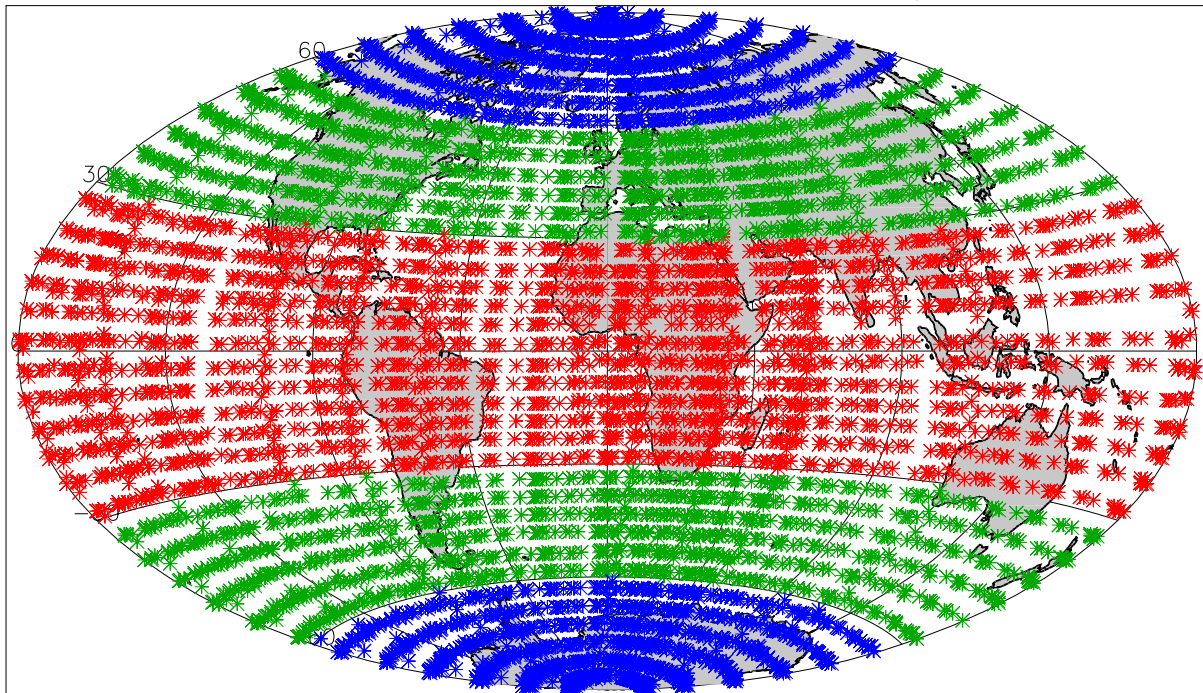


Figure 3.6: Distribution of 6561 temperature profiles retrieved by IMK (product version 1.0) from operational ESA level 1b MIPAS data. Period: Sep 8, 12, 14–28, Oct 11–13, 2002. The whole sample is separated into three latitude bands: low (-30° to $+30^{\circ}$, 2118 events), middle ($\pm 30^{\circ}$ to $\pm 60^{\circ}$, 2151 events), and high ($\pm 60^{\circ}$ to $\pm 90^{\circ}$, 2292 events).

The MIPAS-temperature profiles used for comparison with CHAMP profiles in this study are taken from 20 days in September and October 2002 (Sep 8, 12, 14–28, Oct 11–13, see

RO Data and Algorithms Validation Based on CHAMP/GPS Data

CHAMPCLIM – Radio Occultation Data Analysis and Climate Monitoring based on CHAMP/GPS

Fig. 3.6) and are near-equally distributed, except for an increased observational density near the poles.

Out of the 3160 CHAMP and 6561 MIPAS profiles, 184 profiles could be identified as coincidences, most of them occurring at high latitudes. The sparser observational density of both, CHAMP and MIPAS, at low latitudes becomes especially obvious when combining both data sets. Only 16 coincidences take place at low latitudes compared to 41 at mid latitudes and 124 coincidences at high latitudes. The CHAMP/IGAM – MIPAS comparison results are presented in Sect. 4.3.2.

CHAMP–MIPAS coincidences. 2002, Sep 8,12,14–28, Oct 11–13. 184 events

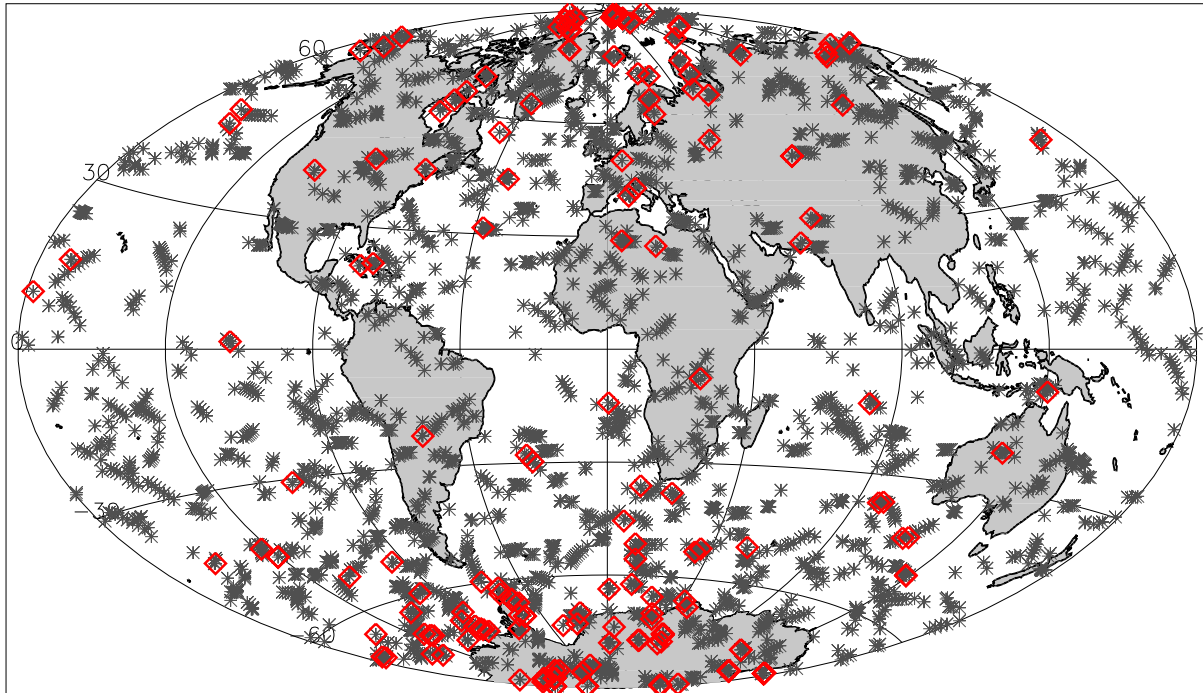


Figure 3.6: Distribution of 3160 CHAMP temperature profiles (black asterisks) in the period Sep 8, 12, 14 – 28, Oct 11 – 13, 2002 and 184 coinciding MIPAS events out of the ensemble 6561 events show in Fig. 3.5 (red diamonds). Coincidence criteria: 300 km / 3 hrs.

GOMOS

The Global Ozone Monitoring by Occultation of Stars instrument (GOMOS) exploits stellar occultation (i.e., the information carried by a star's light when it is modified during its travel through the Earth's atmosphere as the star sets behind the horizon) in the ultraviolet, visible and the near infrared spectral region. The major objective of GOMOS is monitoring of upper tropospheric, stratospheric, and mesospheric ozone, i.e., in the altitude range between 15 and 120 km. GOMOS is additionally equipped with two fast photometers sampling simultaneously the star flux at two wavelengths (around 490 and 675 nm) with a frequency of 1 kHz in order to correct for scintillations in the recorded star spectra. By measuring the time-shift between the "blue" and the "red" photometer, it is possible to determine bending angles caused by density variations of the atmosphere. These bending angles allow for the retrieval of atmospheric temperatures quite similar to the RO retrieval. A preliminary algorithm to derive these "high resolution temperature profiles" (HRTP) was developed by Service d'Aéronomie du CNRS, France. It has been implemented into the GOMOS processing chain, and will be evaluated by comparison with CHAMP-RO temperature profiles in this study (Sect. 4.3.3).

ENVISAT/GOMOS 2002, Sep 20–27, Oct 11–13. 11 days, 1529 events

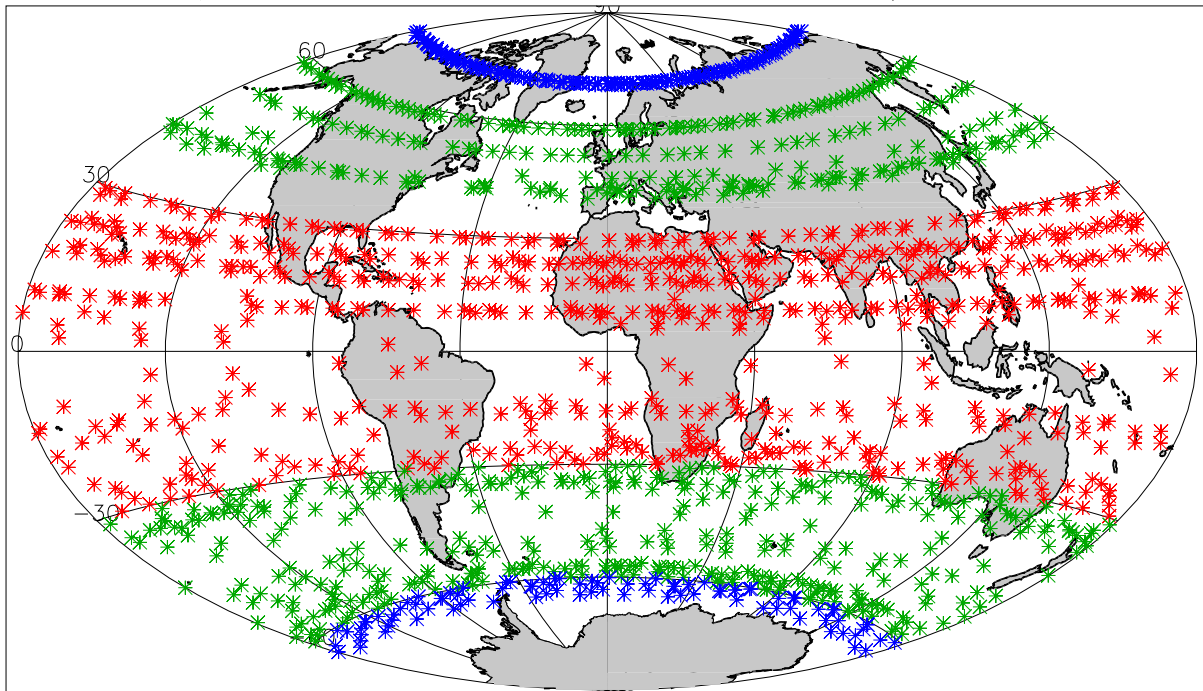


Figure 3.8: Distribution of 1529 high resolution temperature profiles retrieved from GOMOS data. Period: Sep 20 – 27, Oct 11 – 13, 2002. The whole sample is separated into three latitude bands: low (-30° to $+30^\circ$, 644 events), middle ($\pm 30^\circ$ to $\pm 60^\circ$, 625 events), and high ($\pm 60^\circ$ to $\pm 90^\circ$, 260 events).

CHAMP–GOMOS coincidences. 2002, Sep 20–27, Oct 11–13. 32 events

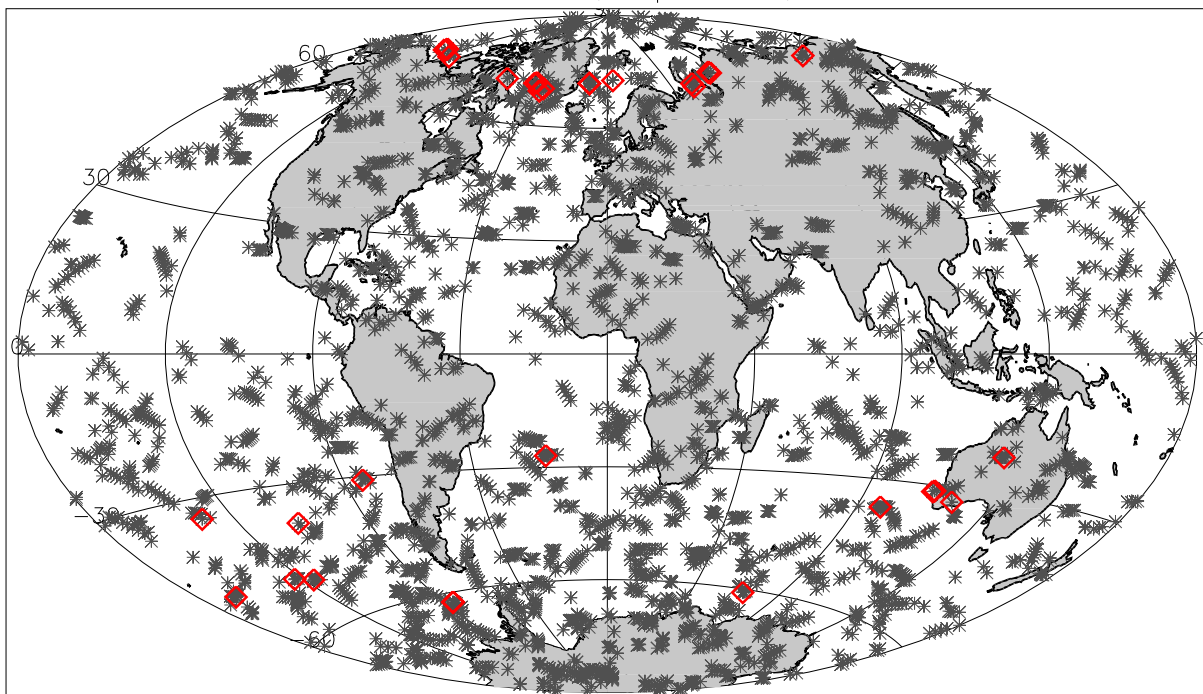


Figure 3.9: Distribution of 1798 CHAMP temperature profiles (black asterisks) from the period Sep 20 – 27, Oct 11 – 13, 2002 and 32 coinciding GOMOS events out of the ensemble of 1529 events show in Fig. 3.8 (red diamonds). Coincidence criteria: 300 km / 3 hrs.

In addition to the H RTP-retrieval, a temperature retrieval based on bending angles profiles extracted from GOMOS star tracker data (SFA/SATU) is under development at IGAM (Retscher et al., 2004). These data products present the movement of the instruments CCD-detector. The star image is kept inside the CCD with a sampling of 100 Hz and errors of 10 μ rad from the central position. Once the bending angle profile and accompanying impact parameters are available, we can apply an inverse Abel transform in a similar way as in the RO retrieval to retrieve atmospheric parameters. First preliminary results of this retrieval algorithm will be evaluated against CHAMP/IGAM temperature profiles in Sect. 4.3.4.

The GOMOS/H RTP and GOMOS/IGAM profiles used for comparison with CHAMP profiles are taken from 11 days in September and October 2002 (Sep 24 – 27, Oct 11 – 13, see Fig. 3.8). Out of the 1592 GOMOS profiles and 1798 CHAMP RO profiles recorded in this period, we identified 32 and 20 coinciding events for the H RTP- and IGAM-retrieval, respectively, using the same coincidence criteria as in the MIPAS study (300 km / 3 hrs). Again, most of the coincidences can be found in the high-latitude region (see Fig. 3.9).

3.2 Validation Methodology

The validation in the following sections is based on error statistics of refractivity and temperature profiles. For each corresponding pair of profiles (\mathbf{x}^{igam} , being an IGAM-retrieved CHAMP profile and \mathbf{x}^{refer} being either a GFZ-operationally retrieved CHAMP profile, an ECMWF profile, or an ENVISAT-MIPAS/GOMOS profile), a difference profile $\Delta\mathbf{x}$ was derived ($\Delta\mathbf{x} = (\Delta x_1, \Delta x_2, \dots, \Delta x_i)^T$ with i denoting the height levels and T the matrix transpose):

$$\Delta\mathbf{x} = (\mathbf{x}^{igam} - \mathbf{x}^{refer}) \quad (3.1)$$

The calculation of the mean of the difference profiles lead to the bias profile \mathbf{b} ,

$$\mathbf{b} = \left[\frac{1}{n} \sum_{k=1}^{k=n} \Delta\mathbf{x}_k \right], \quad (3.2)$$

with n being the number of profiles in the ensemble. Next, the bias was subtracted from each profile giving bias-free profiles $\Delta\mathbf{x}^{biasfree}$,

$$\Delta\mathbf{x}^{biasfree} = \Delta\mathbf{x} - \mathbf{b}. \quad (3.3)$$

From these bias-free profiles we computed the error covariance matrix \mathbf{S} ,

$$\mathbf{S} = \left[\frac{1}{n-1} \sum_{k=1}^{k=n} (\Delta\mathbf{x}_k^{biasfree}) (\Delta\mathbf{x}_k^{biasfree})^T \right], \quad (3.4)$$

with its diagonal elements representing the variances S_{ii} at height level i and with its non-diagonal elements representing the covariances S_{ij} between height level i and j . The square root of its diagonal gives the standard deviation profile \mathbf{s} with:

$$s_i = \sqrt{S_{ii}} \quad (3.5)$$

The root mean square error profiles **rms** writes:

$$rms_i = \sqrt{b_i^2 + s_i^2} \quad (3.6)$$

The error correlation matrix **R** with its elements R_{ij} denotes the error correlation between Δx_i at height i and Δx_j at height j . It is calculated by dividing the covariances S_{ij} by the square root of the variances S_{ii} and S_{jj} :

$$R_{ij} = \frac{S_{ij}}{\sqrt{S_{ii} S_{jj}}} \quad (3.7)$$

Throughout this report temperature differences are given in terms of absolute quantities and refractivity differences in terms of relative quantities. The relative quantities are derived by dividing the absolute quantities by the mean of the reference profiles \mathbf{x}^{refer} at each altitude and are indicated by the subscript rel .

In Sect. 4.3.1, a detailed analysis of the difference between CHAMP and ECMWF refractivity profiles is given, including all quantities described above. All other comparisons are restricted to the absolute bias **b** and the standard deviation **s** (temperature) or relative bias **b_{rel}** and relative standard deviation **s_{rel}** (refractivity), respectively.

4 Validation Results

4.1 Simulation Study

In end-to-end simulation studies, as presented in this section, the errors found can directly be attributed to the simulated observing system and the measurement principle, since no reference data errors as in studies using independent observations or model output occur (i.e., we know “truth” in this case). Only minor representation errors are introduced through comparison of (in general) non-vertical occultation profiles with vertical reference profiles (see Sect. 3.1.3). However, the drawback is that the simulated reality might not contain all aspects contributing to errors in “real-world” measurements.

Fig. 4.1 shows a latitude-height slice of the mean seasonal bias \mathbf{b} of the retrieval scheme implemented in the EGOPS software (“basic IGAM/MSIS-scheme”, left panel). Starting from that, we developed an advanced retrieval scheme (“IGAM/MSIS” as described in Tab. 2.1) focusing on the reduction of biases at high altitudes. A more detailed description of the techniques used to achieve better results at high altitudes will be given in the report on CHAMPCLIM work package 3: “RO Data Processing Advancements for Optimizing Climate Utility”.

The basic IGAM/MSIS scheme (left panel) delivers good results in most regions, but exhibits a significant positive temperature bias in the high-latitude winter region above 25 km, where the used background information (MSISE-90) is known to be biased (Randel et al., 2002). The enhanced IGAM/MSIS scheme (right panel) successfully reduces these biases and clearly improves the retrieval quality in the upper stratosphere. The resulting mean dry temperature field is near bias free (biases < 0.5 K) up to about 40 km.

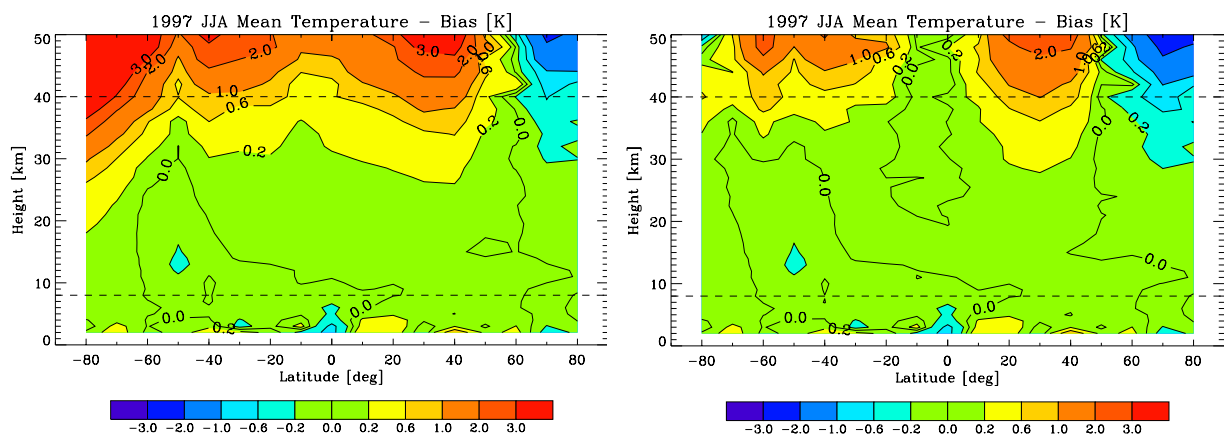


Figure 4.1: Bias \mathbf{b} in the seasonal mean dry temperature for a typical summer season (JJA 1997). Results from the basic IGAM/MSIS scheme (left panel) and from the enhanced IGAM/MSIS scheme as described in Tab. 2.1 (right panel).

4.2 IGAM – GFZ Retrieval Intercomparison

In a retrieval intercomparison study (i.e., the comparison of different retrieval schemes applied to the same set of data), no representation errors occur, but since the retrievals are applied to real CHAMP level 2 data (see Sect. 3.1.2), all “real world” error sources, even those that could not be simulated in the previous study like small-scale structures in the ionosphere, are included here.

This study is an important consistency-check under realistic conditions and additionally allows to judge the effects of different retrieval methods on the retrieved atmospheric profiles. The retrieval schemes under validation were IGAM/MSIS and IGAM/ECMWF (see Sect. 2) compared to GFZ operational, version 4. Since GFZ does not deliver CHAMP level 3 data above 35 km, the validation could not be performed up to 40 km as in the other comparisons presented in this report.

Refractivity

Figs. 4.2 and 4.3 show relative bias \mathbf{b}_{rel} (bold line) and rel. bias \pm rel. standard deviation profiles $\mathbf{b}_{rel} \pm \mathbf{s}_{rel}$ (light lines) of refractivity retrieved with the IGAM/MSIS and the IGAM/ECMWF schemes relative to GFZ operational retrieval results (IGAM – GFZ) for the global ensemble (left panel) and for the latitudinal separated ensembles in the three following panels. Both IGAM retrieval schemes are, compared to GFZ, virtually bias-free below 25 km in all latitude bands (a slight bias of $\sim 0.2\%$ exists in the mid-latitude ensemble). \mathbf{s}_{rel} amounts $\sim 0.5\%$ below 16 km and $\sim 1.1\%$ above that up to ~ 33 km in the IGAM/MSIS case and up to ~ 30 km in the IGAM/ECMWF case. An additional increase above 33 (30) km is due to data in the high-latitude sample.

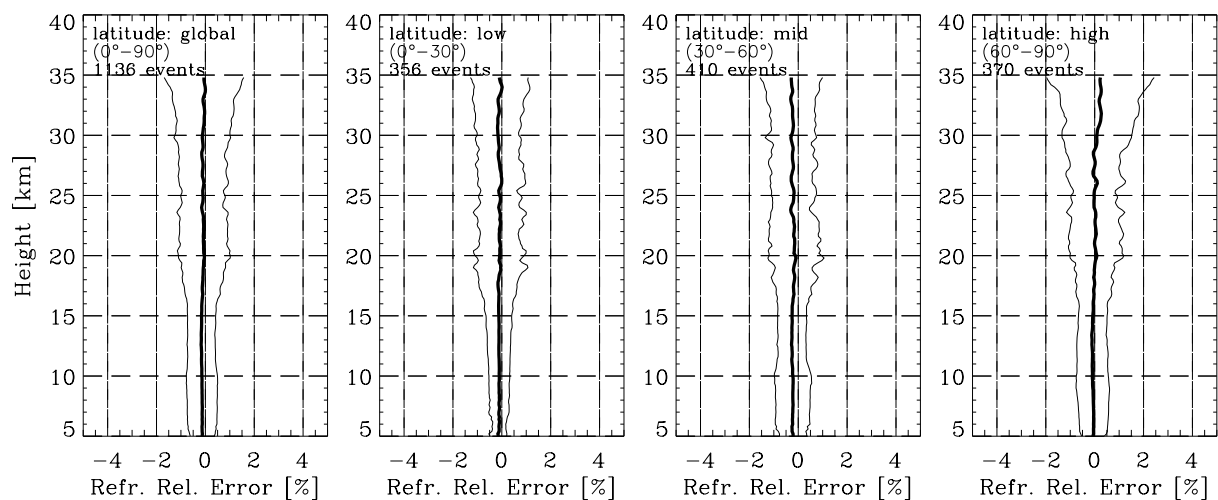


Figure 4.2: Relative bias \mathbf{b}_{rel} (bold) and rel. bias \pm rel. standard deviation profiles $\mathbf{b}_{rel} \pm \mathbf{s}_{rel}$ (light) of refractivity retrieved from CHAMP level 2 data with the IGAM/MSIS scheme relative to operational GFZ (version 4) results. Left panel: global ensemble (1136 occultation events), middle-left panel: low-latitude ensemble (356 events), middle-right panel: mid-latitude ensemble (410 events), right panel: high-latitude ensemble (370 events).

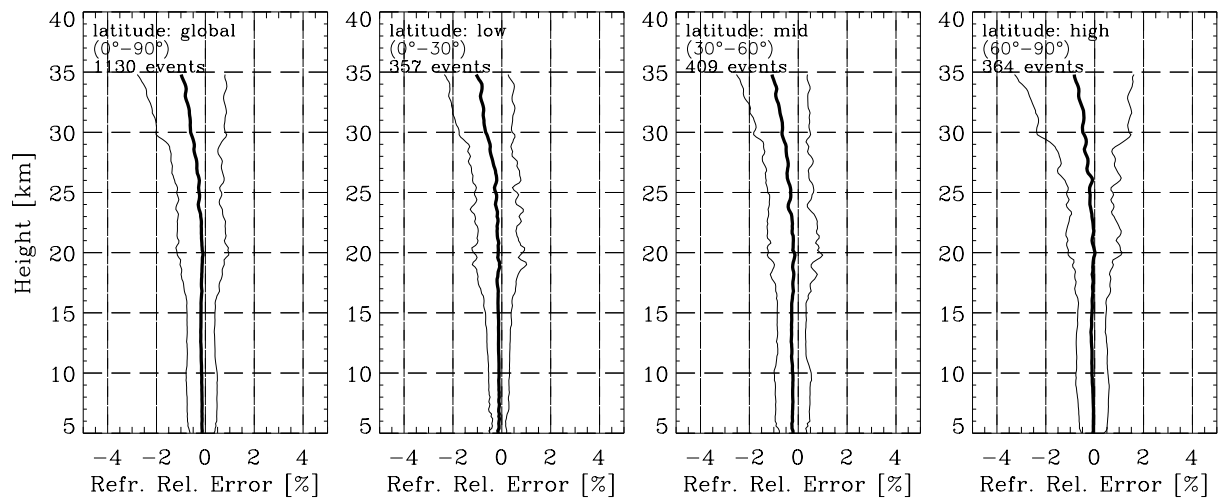


Figure 4.3: Relative bias b_{rel} (bold) and rel. bias \pm rel. standard deviation profiles $b_{rel} \pm s_{rel}$ (light) of refractivity retrieved from CHAMP level 2 data with the IGAM/ECMWF scheme relative to operational GFZ (version 4) results. Left panel: global ensemble (1130 occultation events), middle-left panel: low-latitude ensemble (352 events), middle-right panel: mid-latitude ensemble (409 events), right panel: high-latitude ensemble (364 events).

Temperature

Figs. 4.4 and 4.5 show b and $b \pm s$ profiles of dry temperature retrieved with the IGAM/MSIS and the IGAM/ECMWF schemes, respectively, compared to GFZ operational retrieval results.

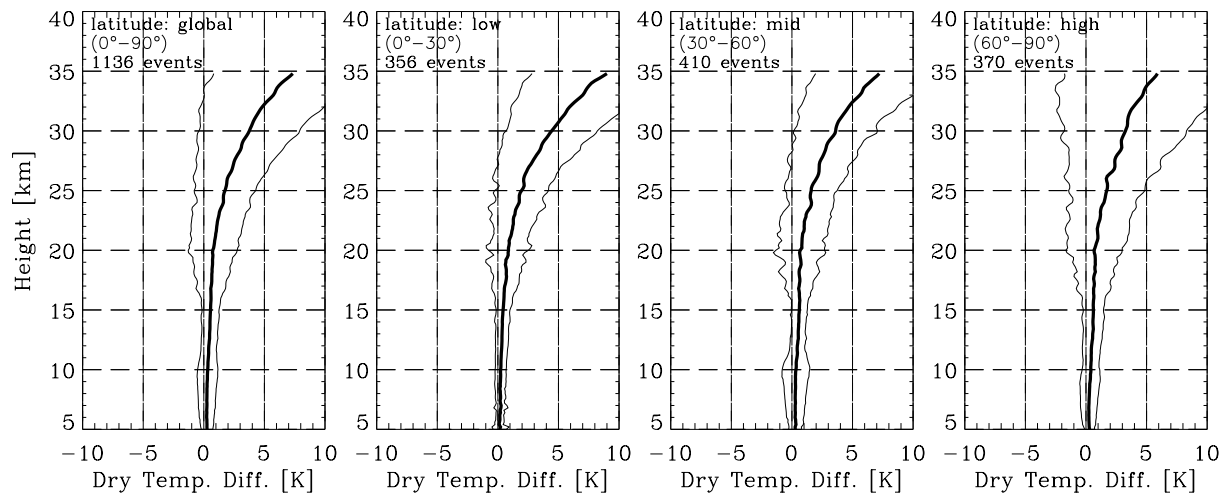


Figure 4.4: Bias b (bold) and bias \pm standard deviation profiles $b \pm s$ (light) of dry temperature retrieved from CHAMP level 2 data with the IGAM/MSIS scheme relative to operational GFZ (version 4) results. Left panel: global ensemble (1136 occultation events), middle-left panel: low-latitude ensemble (356 events), middle-right panel: mid-latitude ensemble (410 events), right panel: high-latitude ensemble (370 events).

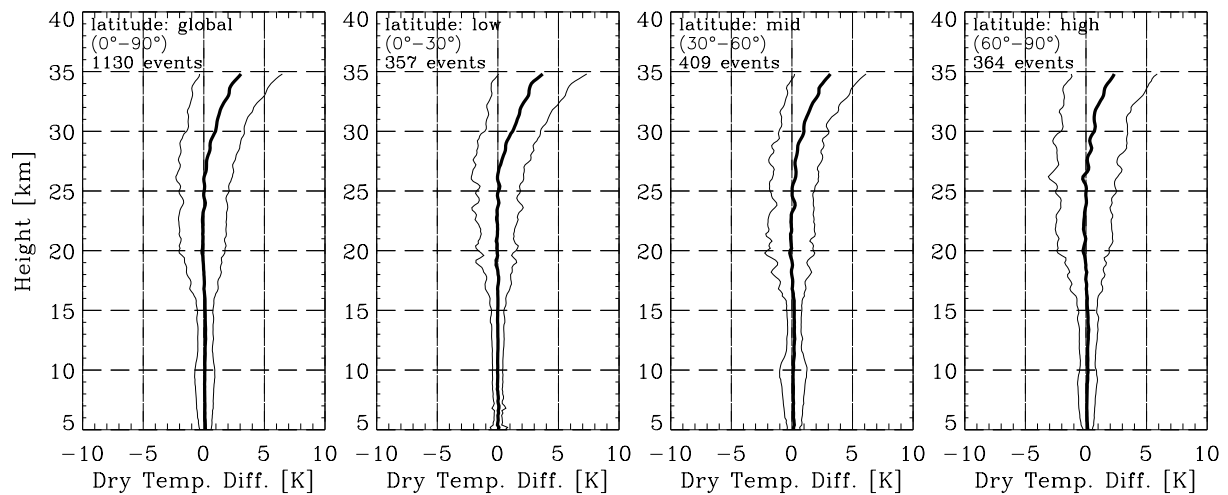


Figure 4.5: Bias **b** (bold) and bias \pm standard deviation profiles **b** \pm **s** (light) of dry temperature retrieved from CHAMP level 2 data with the IGAM/ECMWF scheme relative to operational GFZ (version 4) results. Left panel: global ensemble (1130 occultation events), middle-left panel: low-latitude ensemble (352 events), middle-right panel: mid-latitude ensemble (409 events), right panel: high-latitude ensemble (364 events).

The IGAM/MSIS dry temperatures in the global ensemble are virtually unbiased relative to the GFZ results between 5 and 10 km, positively biased in the order of 0.1 K between 10 and 20 km and positively biased above that, starting with 1 K at ~21 km and increasing to 7 K at 35 km. In opposition to that, the IGAM/ECMWF temperatures are unbiased up to 27 km relative to the GFZ dry temperatures. Above 27 km, a positive bias increasing up to 3 K at 35 km occurs. The standard deviations amount to ~0.5 K below 16 km in both cases and increase up to 6 K and 3 K at 35 km, respectively. Except from slight variations, the description of the global ensemble applies to the latitudinal separated ensembles as well.

Interpretation of the IGAM-GFZ Intercomparison Results

One significant feature of this intercomparison is the standard deviation “jump” at 16 km. Other validation studies (e.g., Wickert et al., 2004a) imply that the major part of the variation between 16 and 30 km is due to increased variance in the IGAM data set. Tests showed that stronger removal of vertical fluctuations of bending angles during the ionospheric correction procedure as described by Hocke et al. (2003) can reduce the standard deviation, but introduces a positive temperature bias above 30 km. Since the IGAM retrieval schemes are aiming to produce high-quality data for climate applications where bias-free data is most important, we decided to accept a more pronounced variance in the data set in order to avoid biases.

The behavior of the IGAM-biases relative to GFZ can be explained by different background data used and different methods of integrating these data into the retrieval. This topic will be partly addressed in Sect. 4.3 and in the conclusions (Sect. 5). A detailed discussion would be beyond the scope of this report and will be part of the report on CHAMPCLIM work package 3: “RO Data Processing Advancements for Optimizing Climate Utility“. Details on the IGAM retrieval schemes and on the methods of optimizing the retrieval using background information can additionally be found in Gobiet and Kirchengast (2004) and Gobiet et al. (2004).

4.3 Validation with Independent Data Sources

When comparing CHAMP occultation data with independent data sources, the derived error estimates represent a combined estimate of the observation errors of both instruments, or the ECMWF model error, respectively, and of the representation error. The representation error stems from the spatial distance and the time delay between two observations, the limited horizontal resolution of limb-viewing remote sensing methods, and the limited spatial and temporal model resolution in the ECMWF-case. Additionally, the comparison of differently orientated slant profiles with each other or with vertical ECMWF-derived profiles can cause representation errors.

In general, the average zenith angle of the tangent point trajectory of RO profiles near the Earth's surface is about 85° . This fact, and the other reasons for representation errors become important in the lower troposphere, below ~ 7 km, when high horizontal variability is present in the atmosphere (Foelsche and Kirchengast 2003; Syndergaard et al. 2003). Since we will not interpret results in the lower troposphere, this aspect of the representation error is negligible. The representation error due to different vertical resolution of the compared profiles can not be neglected, however.

4.3.1 ECMWF-NWP analyses

Refractivity

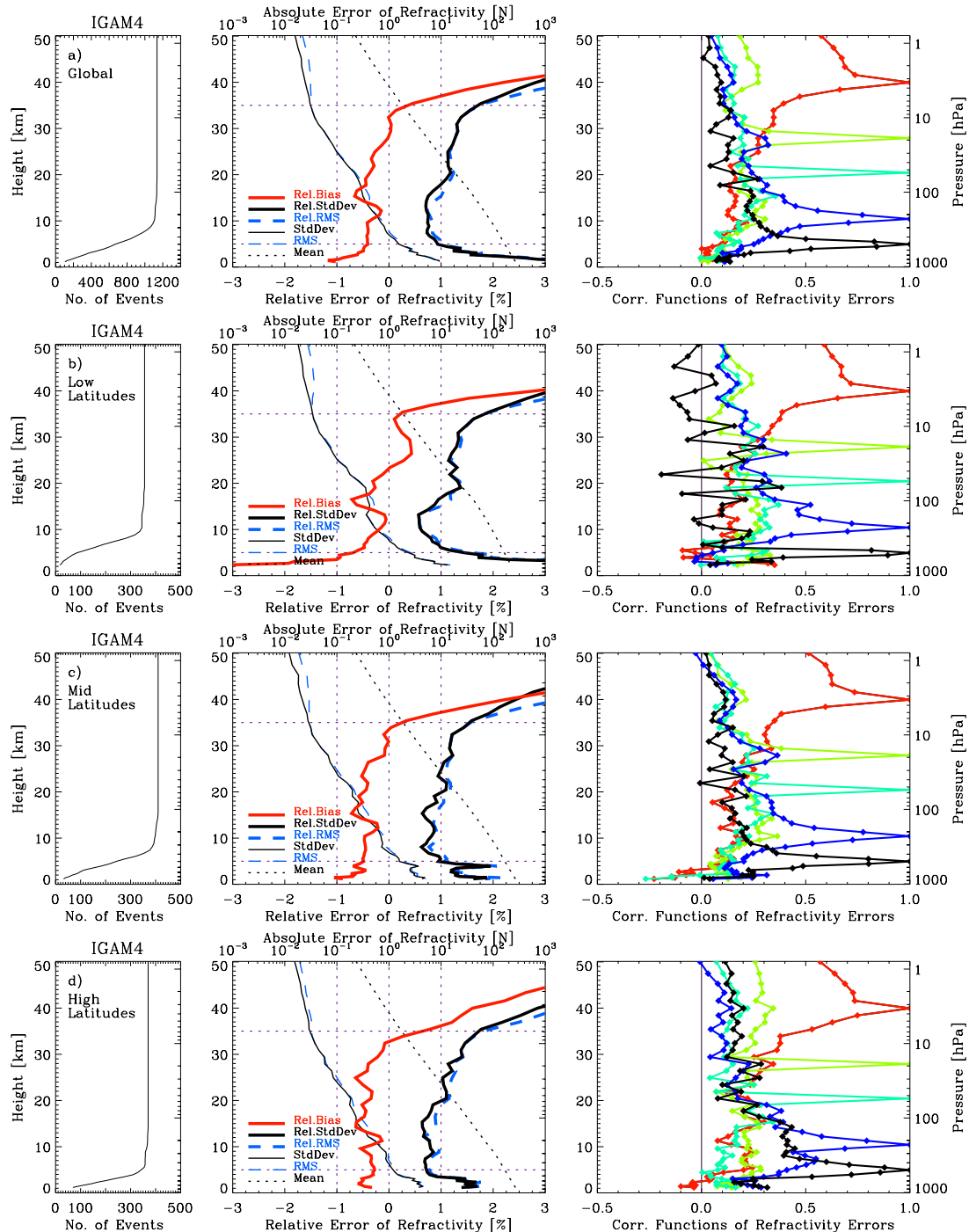


Figure 4.6: IGAM/MSIS – ECMWF refractivity error analysis results for the global (a) and the latitudinal separated ensembles (b – d). Left panels: number of events used for the error statistics calculation at any given height. Middle panels: relative bias (bold, red), relative standard deviation (bold, black), relative rms (bold, blue, dashed) as well as the absolute standard deviation (light black), absolute rms (light blue, dashed), and the mean of the reference profiles (dotted). Right panels: error correlation functions for ~ 40 km, ~ 30 km, ~ 20 km, ~ 10 km, and ~ 5 km height, representative of upper stratosphere, lower stratosphere, and troposphere, respectively.

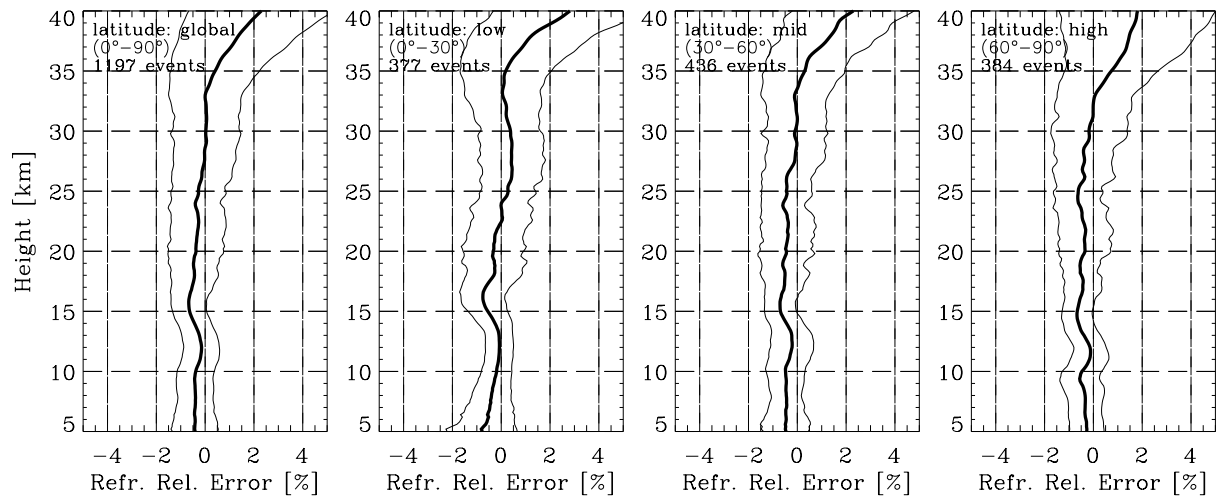


Figure 4.7: Relative bias \mathbf{b}_{rel} (bold) and rel. bias \pm rel. standard deviation profiles $\mathbf{b}_{rel} \pm \mathbf{s}_{rel}$ (light) of refractivity retrieved from CHAMP level 2 data with the IGAM/MSIS scheme relative to data derived from co-located ECMWF operational analyses. Left panel: global ensemble (1197 occultation events), middle-left panel: low-latitude ensemble (377 events), middle-right panel: mid-latitude ensemble (436 events), right panel: high-latitude ensemble (384 events).

The refractivity error estimates based on the empirical error analyses of the IGAM/MSIS (Fig. 4.6) and the IGAM/ECMWF retrieval (Fig. 4.8) compared to ECMWF analyses are depicted for the global (panels a) and latitudinal separated ensembles (panels b – d). The left small panels show the number of events entering the statistics. The middle panels illustrate the error characteristics comprising bias \mathbf{b} , standard deviation \mathbf{s} , and root mean square profiles \mathbf{rms} in terms of absolute quantities (light lines) shown at the upper abscissa and in terms of relative quantities (bold lines) displayed at the lower abscissa. The domain of main interest for the interpretation of the results is 5 – 35 km, indicated by the dotted lines. The right panels display the error correlation functions for different height levels (~ 40 km, ~ 30 km, ~ 20 km, ~ 10 km, and ~ 5 km) representative of upper stratosphere, lower stratosphere, and troposphere. The error correlation functions are defined as the rows of the error correlation matrix \mathbf{R} (Eq. 3.7). These functions express the correlation of errors at these heights with the errors in the remainder of the profile.

For the sake of better comparability with other results presented in this report, the refractivity profile relative error statistics are additionally shown in a simpler format as used in the other sections. In these figures, \mathbf{b}_{rel} (bold line) and $\mathbf{b}_{rel} \pm \mathbf{s}_{rel}$ profiles (light lines) are depicted. Fig. 4.7 shows the IGAM/MSIS retrieval and Fig. 4.9 the IGAM/ECMWF retrieval, both compared to co-located ECMWF analyses.

It must be noted that for the IGAM/MSIS retrieval ECMWF-analyses can be regarded as independent validation data, but the IGAM/ECMWF retrieval is not independent from ECMWF at high altitudes as explained in Sect. 2.2. For this reason, this comparison can not be interpreted as a validation for the IGAM/ECMWF retrieval algorithm, but gives important insights in the retrieval performance.

Figs. 4.6 and 4.7 exhibit the results of the IGAM/MSIS refractivity retrieval with respect to ECMWF analysis profiles. In the global, as well as in the mid- and high latitude ensembles \mathbf{b}_{rel} oscillates around -0.4% below 25 km while it ranges from -0.75 to 0% in low latitudes. In all ensembles, especially in the global mean, \mathbf{b}_{rel} approaches 0% in the 25 – 35 km range and drastically increases to levels $> 3\%$ above that.

s_{rel} stays below 1 % at 5 – 20 (18) km height in mid- and high (low) latitudes and in the global mean, varies around 1.2 % up to 32 km and drastically increases above that to levels > 3 % in all ensembles.

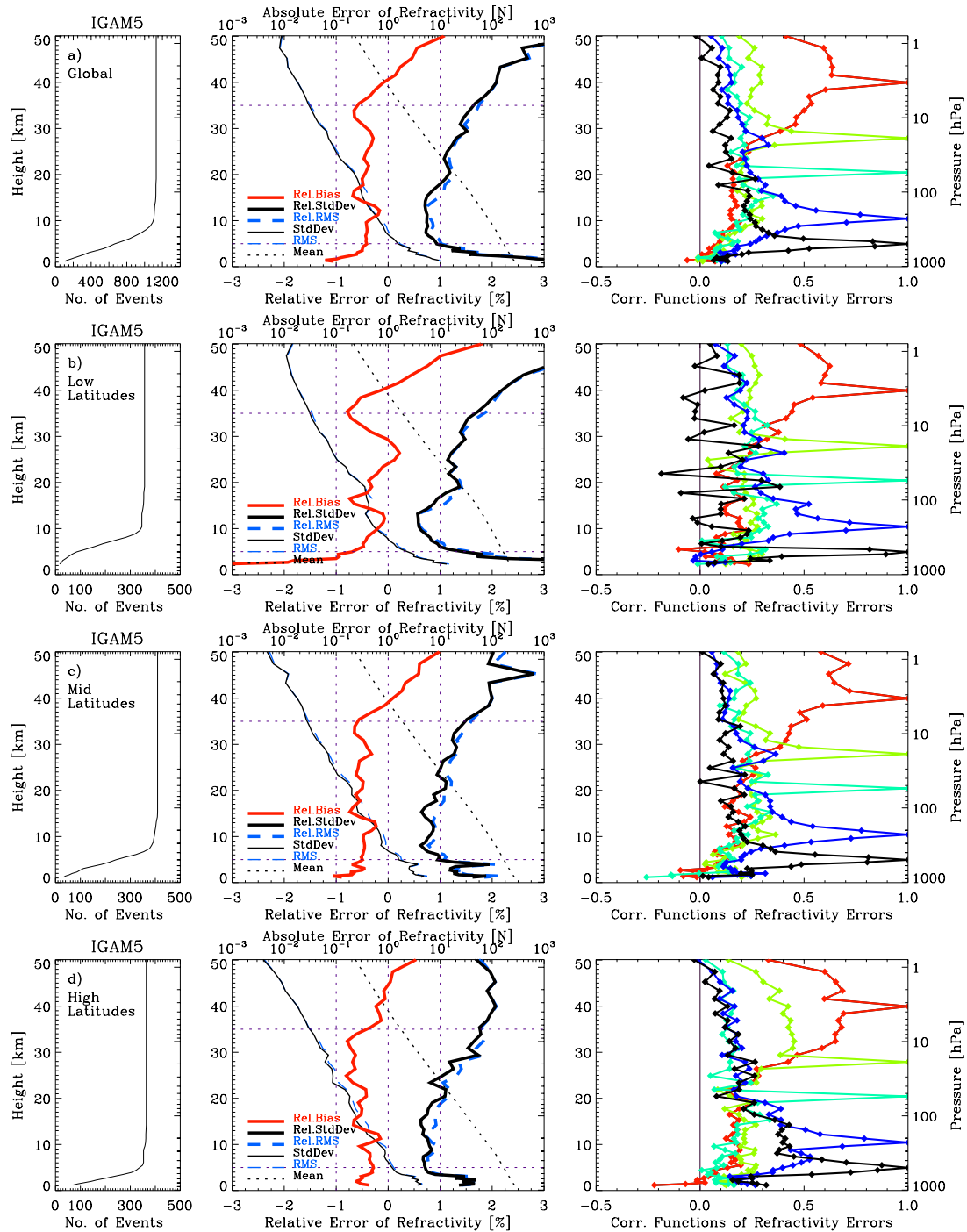


Figure 4.8: IGAM/ECMWF – ECMWF refractivity error analysis results for the global (a) and the latitudinal separated ensembles (b – d). Left panels: number of events used for the error statistics calculation at any given height. Middle panels: relative bias (bold, red), relative standard deviation (bold, black), relative rms (bold, blue, dashed) as well as the absolute standard deviation (light black), absolute rms (light dashed), and the mean of the reference profiles (dotted). Right panels: error correlation functions for ~ 40 km, ~ 30 km, ~ 20 km, ~ 10 km, and ~ 5 km height, representative of upper stratosphere, lower stratosphere, and troposphere, respectively.

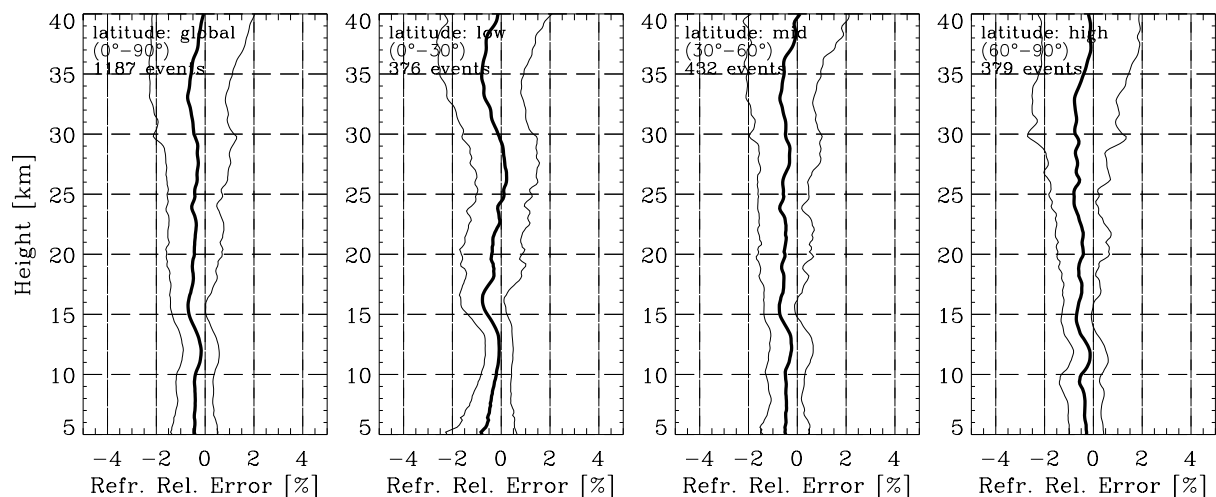


Figure 4.9: Relative bias b_{rel} (bold) and rel. bias \pm rel. standard deviation $b_{rel} \pm s_{rel}$ (light) of refractivity retrieved from CHAMP level 2 data with the IGAM/ECMWF scheme relative to data derived from co-located ECMWF operational analyses. Left panel: global ensemble (1187 occultation events), middle-left panel: low-latitude ensemble (376 events), middle-right panel: mid-latitude ensemble (432 events), right panel: high-latitude ensemble (379 events).

Figs. 4.8 and 4.9 exhibit the results of the IGAM/ECMWF refractivity retrieval with respect to ECMWF analysis profiles. In the global, as well as in the latitudinal separated ensembles, b_{rel} oscillates around -0.4% (with stronger fluctuations in the low-latitude ensemble) up to 35 km which is 10 km higher as in the IGAM/MSIS-case. Above 35 km, b_{rel} increases drastically, though less drastic than in the IGAM/MSIS-case, and does not exceed 1% up to 50 km.

s_{rel} stays below 1% at 5–20 (18) km height in mid- and high (low) latitudes and in the global mean, varies around 1.2% up to 30 km to increase above that to $\sim 3\%$ at 50 km. Compared to the IGAM/MSIS retrieval, s_{rel} is significantly smaller above 35 km.

Interpretation of the Refractivity Results

As mentioned before, the comparison of IGAM/ECMWF retrieved refractivities with ECMWF-derived data can not be regarded as a validation since the background information used in the retrieval is the same as the reference data. However, the influence of the two very different sources of background information used in a very different way in the retrieval (MSISE-90 climatology as a search library of representative states of the atmosphere, and co-located ECMWF analyses, respectively) can be compared this way.

Generally, a constant negative refractivity bias of -0.4% exists up to 35 km in the IGAM/ECMWF retrieval. In the IGAM/MSIS retrieval results, a similar bias exists below 25 km, it approaches zero above that altitude, and crosses the zero-line at ~ 35 km to drastically increase from there on upwards. Since the IGAM/ECMWF retrieval results are optimized towards the ECMWF analyses at high altitudes (the transition height from background-dominated to observation-dominated lies at some 50 km in the refractivity profile), we can not conclude that the IGAM/MSIS retrieval performs better between 25 and 35 km. Quite contrary, the negative refractivity bias seems to be constant with height and is only masked by the declining data quality above 25 km in the case of the IGAM/MSIS-retrieval. This is probably caused by a not yet clearly identified inconsistency in the altitude allocation of either the retrieved, or the reference data. A similar bias compared to ECMWF analyses, at least up to 25 km, can be found in the RO-derived refractivities of other leading

institutions in the field of RO-retrieval (GFZ, Danish Meteorological Institute (DMI); Steiner, 2004; Wickert et al., 2004a; Beyerle et al., 2004). At high altitudes (above 25 and 35 km, respectively), this bias is masked by the increasing measurement errors and the rising influence of background information.

The comparison of the bias-profiles of both IGAM retrieval schemes indicates that the refractivity profiles derived by the IGAM/ECMWF-scheme are virtually background-independent and, apart from the minor height-constant bias mentioned before, unbiased below 35 km. The same conclusion can be drawn for the IGAM/MSIS results below 25 km and, if biases in the order of 0.1 % are acceptable, below 35 km. Above 35 km, the IGAM/MSIS results can not be regarded to yield useful observed information. The IGAM/ECMWF results might be useful up to higher altitudes, but no clear conclusions about that can be drawn from this study.

A further salient feature in Figs. 4.6 – 4.9 is the wave-shaped structure in the bias profile between 10 and 20 km that is present in all ensembles regardless of the retrieval scheme applied. This structure can also be found in the temperature error profiles (see next subsection) and will be discussed there.

Temperature

Figs. 4.10 and 4.11 show \mathbf{b} and $\mathbf{b} \pm \mathbf{s}$ profiles of dry temperature retrieved with the IGAM/MSIS and the IGAM/ECMWF schemes, respectively, with respect to ECMWF analysis profiles.

The IGAM/MSIS temperature error statistics in the global ensemble show qualitatively similar features as the error statistics relative to the GFZ-operational dry temperatures: Virtually no bias between 5 and 10 km, a positive bias in the order of 0.1 K between 10 and 20 km and a positive bias above that height, starting with 1 K at ~ 20 km and increasing to 6 K at 35 km. The IGAM/ECMWF dry temperatures are unbiased up to ~ 30 km, above, a warm bias of about 1.5 K occurs. The standard deviations amount to 1 – 2 K below 16 km and increase up to ~ 2.5 K in 25 km in both cases. Above that, the IGAM/MSIS standard deviation increases drastically while the IGAM/ECMWF values stay below 3 K up to 35 km. Except from slight variations, the description of the global ensemble applies to the latitudinal separated ensembles as well.

For both retrieval-schemes, a wave-shaped structure between 8 and 18 km occurs in the bias profile, being at lowest altitudes in the high-latitude ensemble and at highest altitudes in the low-latitude ensemble.

Interpretation of the Temperature Results

The strong warm high-altitude bias of the IGAM/MSIS retrieved dry temperatures compared to co-located ECMWF temperatures (as well as compared to the GFZ dry temperatures) shows that this retrieval scheme, applied to CHAMP data yields biased results in the order of 1 K and bigger above 20 km. This shows that the background bias correction algorithm involved is not fully effective when applied to CHAMP data. Due to the fact that the IGAM/MSIS scheme was successfully evaluated in simulation studies using METOP-GRAS receiver specifications (Gobiet and Kirchengast, 2004), the lacking performance applied to CHAMP data indicates that worse data quality at high altitudes (higher receiver-noise level, outliers, residual ionospheric noise stemming from small-scale structures in the ionosphere that were not modeled in the simulation study), prevents the scheme from being successful.

In opposition to that, the IGAM/ECMWF dry temperatures are virtually unbiased against ECMWF analyses below 30 km and slightly warm biased above that. The most interesting

RO Data and Algorithms Validation Based on CHAMP/GPS Data

CHAMPCLIM – Radio Occultation Data Analysis and Climate Monitoring based on CHAMP/GPS

feature of this comparison (since it can not be used as validation for the retrieval scheme) is, that though ECMWF temperatures were used as background information in the retrieval and as reference data, the retrieval results differ from it at high altitudes where the influence of the background is strongest. This indicates that the retrieval is not dominated by the background at least down to 40 km which makes it a potentially valuable observation up to this altitude. The discrepancy between IGAM/ECMWF temperatures and ECMWF analysis temperatures is not necessarily a deficiency of the observation since ECMWF is known to be cold biased above 30 km by ~ 0.8 K and is hardly constrained by observations at this altitude.

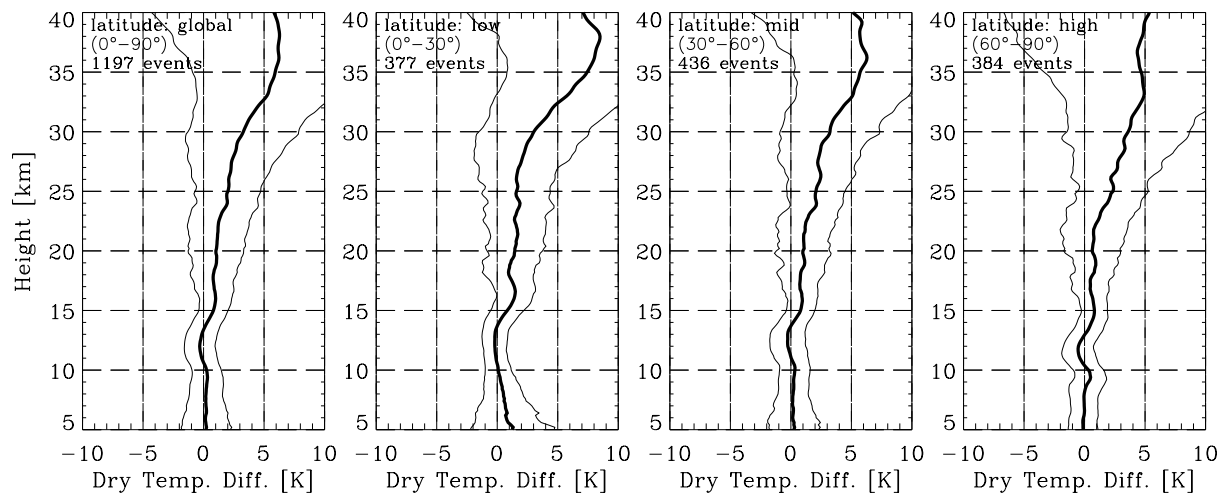


Figure 4.10: Bias b (bold) and bias \pm standard deviation profiles $b \pm s$ (light) of dry temperature retrieved from CHAMP level 2 data with the IGAM/MSIS scheme relative to temperatures derived from co-located ECMWF operational analyses. Left panel: global ensemble (1197 occultation events), middle-left panel: low-latitude ensemble (377 events), middle-right panel: mid-latitude ensemble (436 events), right panel: high-latitude ensemble (384 events).

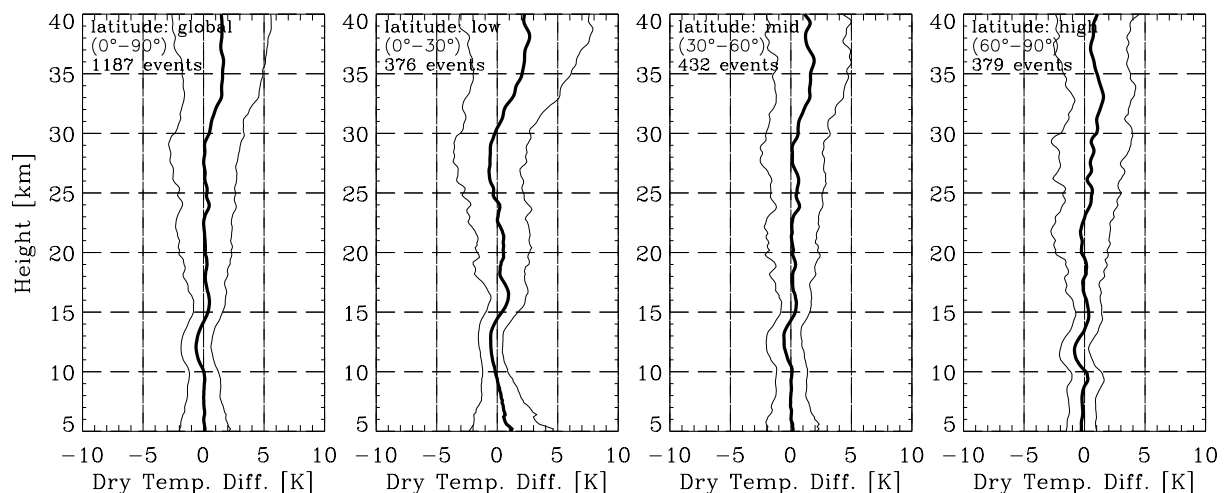


Figure 4.11: Bias b (bold) and bias \pm standard deviation profiles $b \pm s$ (light) of dry temperature retrieved from CHAMP level 2 data with the IGAM/ECMWF scheme relative to temperatures derived from co-located ECMWF operational analyses. Left panel: global ensemble (1187 occultation events), middle-left panel: low-latitude ensemble (376 events), middle-right panel: mid-latitude ensemble (432 events), right panel: high-latitude ensemble (379 events).

Wave-shaped structures in the dry temperature bias profiles (between 8 and 18 km) are found ~ 2 km lower than similar structures in the refractivity bias profiles. This is in accordance with the retrieval procedure, since the involved hydrostatic integration (Eq. 2.3) causes downward-propagation of information. The altitude of the structures lies in the tropopause-region and its shape indicates that these features are caused by the different effective vertical resolution of the CHAMP-RO profiles and the ECMWF reference profiles (small-scale structures being better captured by CHAMP-RO profiles). In order to demonstrate this situation, a single CHAMP-RO profile and its collocated profile derived from the ECMWF analysis, along with the difference of these two profiles is shown in Fig. 4.12. Further examples can be found in Appendix B.

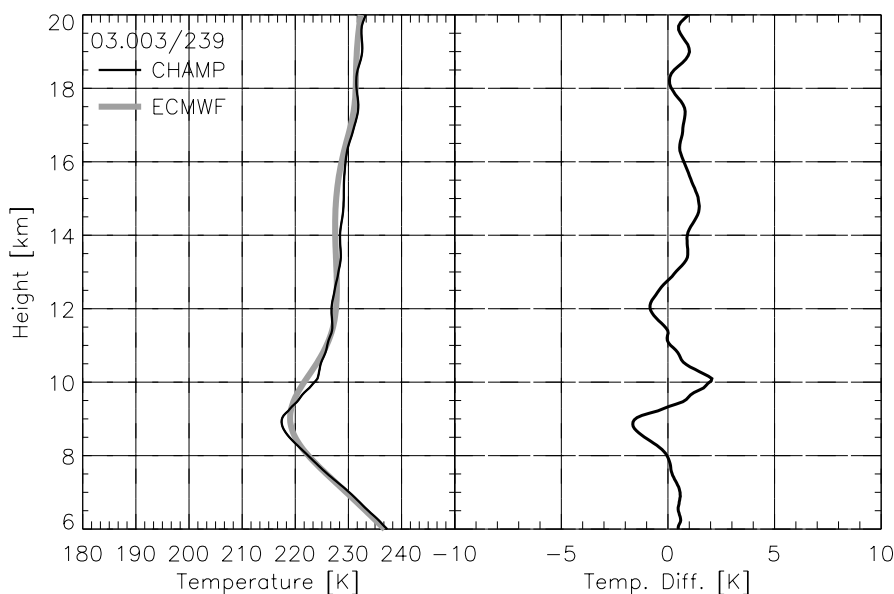


Figure 4.12: Temperature profile derived from CHAMP (-73.9° latitude, -38.3° longitude, Jan 3, 2003, 22:10 UT, IGAM/ECMWF retrieval) compared to collocated temperatures from ECMWF operational analyses. Left panel: temperature profiles. Right panels: Difference $T_{\text{CHAMP}} - T_{\text{ECMWF}}$.

4.3.2 MIPAS

Temperature Comparison

Figs. 4.13 and 4.14 show \mathbf{b} and $\mathbf{b} \pm \mathbf{s}$ profiles of dry temperature retrieved with the IGAM/MSIS and the IGAM/ECMWF schemes, respectively, with respect to ENVISAT/MIPAS temperature profiles. The IGAM/MSIS temperature error statistics are not discussed since the main conclusions drawn in the previous section qualitatively apply here as well. Characteristic features according to the MIPAS instrument are discussed by means of the IGAM/ECMWF error statistics (Fig. 4.14).

In the global and the latitudinal separated ensembles, there is virtually no bias between 6 and 25 km, between 25 and 35 km a cold bias of about 1 K peaking at ~ 30 km (2 K) exists. Between 30 and 37 km the bias vanishes again. The standard deviation in the global ensemble is height-constant and amounts to ~ 3 K. The low- and mid-latitude ensembles feature smaller standard deviations though, this can not be interpreted easily since the sample-size in these

ensembles is very small (16 and 41 events, respectively). The major contribution to the global error statistics stems from the high-latitude ensemble comprising 127 events.

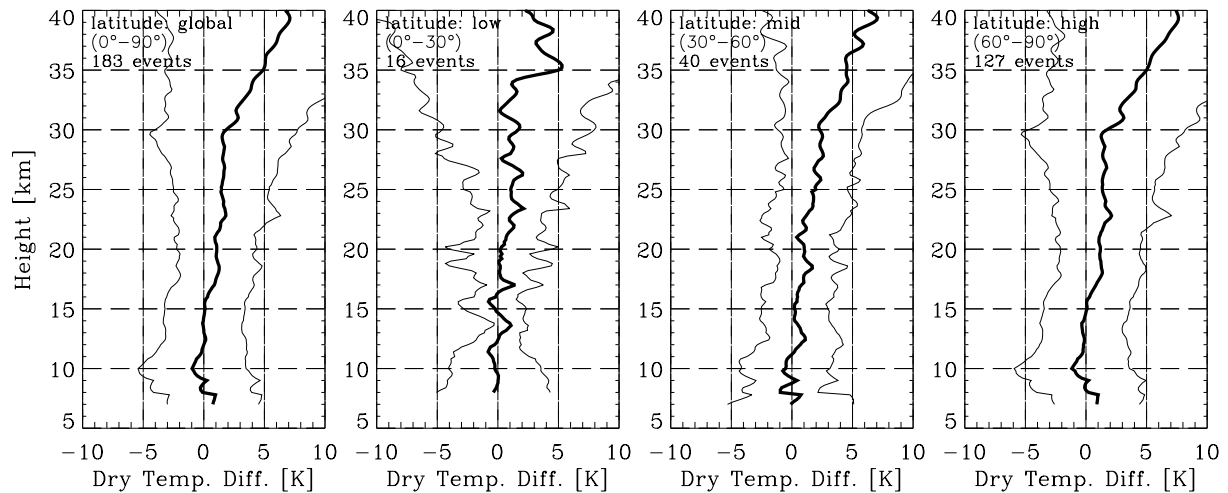


Figure 4.13: Bias b (bold) and bias \pm standard deviation profiles $b \pm s$ (light) of dry temperature retrieved from CHAMP level 2 data with the IGAM/MSIS scheme relative to coinciding temperature profiles from ENVISAT/MIPAS. Coincidence-criteria: 300 km / 3 hrs. Left panel: global ensemble (183 events), middle-left panel: low-latitude ensemble (16 events), middle-right panel: mid-latitude ensemble (40 events), right panel: high-latitude ensemble (127 events).

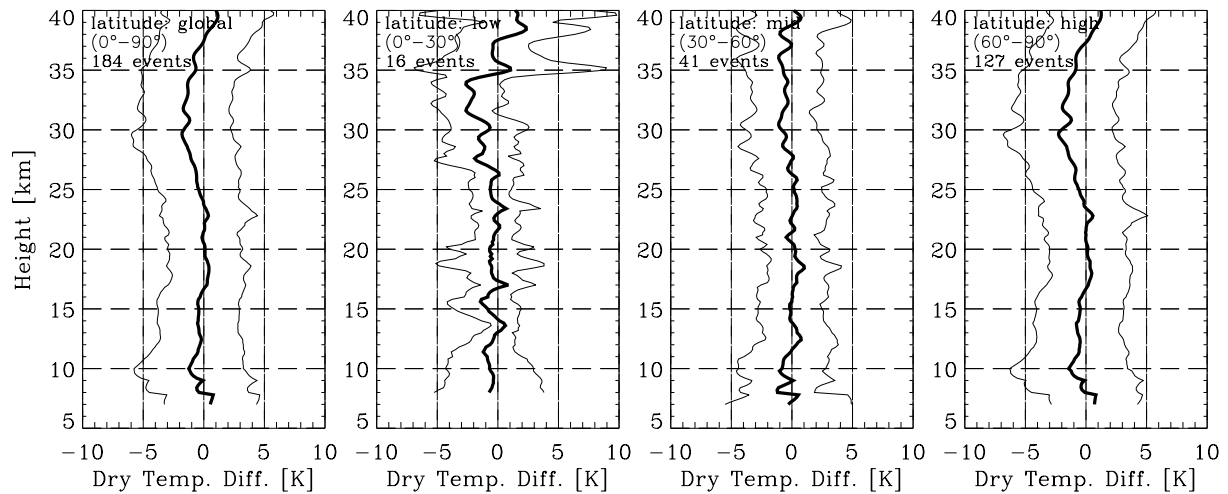


Figure 4.14: Bias b (bold) and bias \pm standard deviation profiles $b \pm s$ (light) of dry temperature retrieved from CHAMP level 2 data with the IGAM/ECMWF scheme relative to coinciding temperature profiles from ENVISAT/MIPAS. Coincidence-criteria: 300 km / 3 hrs. Left panel: global ensemble (184 events), middle-left panel: low-latitude ensemble (16 events), middle-right panel: mid-latitude ensemble (41 events), right panel: high-latitude ensemble (127 events).

Interpretation

The near-height independent standard deviation of ~ 3 K of the IGAM/ECMWF – MIPAS error statistics can be mainly contributed to the variance in the MIPAS data set, since in the previous sections and in other studies (e.g. Hajj et al., 2003) the RO technique and the IGAM-retrieval schemes were shown to exhibit a standard deviation of < 2 K below 25 km. Above that, both data sets may contribute in equal parts.

The most interesting result of this comparison is the fact that the IGAM/ECMWF temperatures are not warm biased against MIPAS temperatures above 30 km as it is the case in the comparisons with ECMWF analyses. Since MIPAS is nearly independent from ECMWF (see Sect. 3.1.4) this is a strong argument for the reliability of the CHAMP derived temperature of the IGAM/ECMWF-scheme above 30 km as well.

4.3.3 GOMOS HRTP

Figs. 4.15 and 4.16 show \mathbf{b} and $\mathbf{b} \pm \mathbf{s}$ profiles of dry temperature retrieved with the IGAM/MSIS and the IGAM/ECMWF schemes, respectively, with respect to GOMOS/HRTP temperature profiles (see Sect. 3.1.4). Due to lacking quality of GOMOS data below 20 km, only the height interval from 20–40 km is shown. Apart from GOMOS-characteristic features that will be discussed by means of the IGAM/ECMWF – GOMOS/HRTP error statistics, the IGAM/MSIS – GOMOS/HRTP error statistics roughly feature the main characteristic of the IGAM/MSIS error-statistics relative to other data sources, namely a significant positive bias in the middle stratosphere.

Temperature Comparison

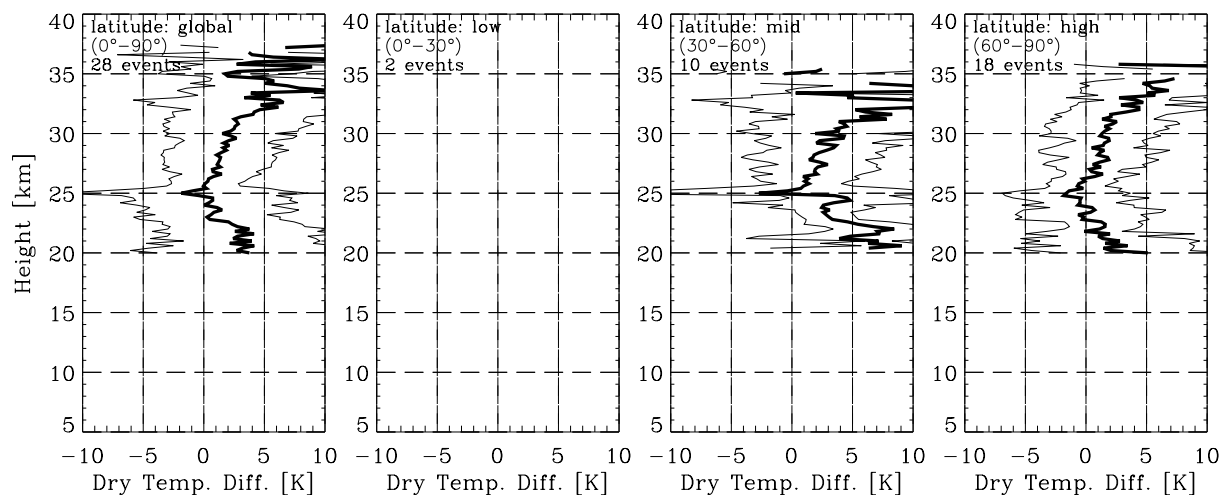


Figure 4.15: Bias \mathbf{b} (bold) and bias \pm standard deviation profiles $\mathbf{b} \pm \mathbf{s}$ (light) of dry temperature retrieved from CHAMP level 2 data with the IGAM/MSIS scheme relative to coinciding GOMOS/HRTP temperature profiles. Coincidence-criteria: 300 km / 3 hrs. Left panel: global ensemble (28 events), middle-left panel: low-latitude ensemble (2 events, no error statistics possible), middle-right panel: mid-latitude ensemble (10 events), right panel: high-latitude ensemble (18 events). The discrepancy in the sample sizes is due to the fact that in some GOMOS-profiles only few data-points are available. The number of available profiles is defined as the maximum number of data points at all altitude levels which can be smaller than the sum of the profiles.

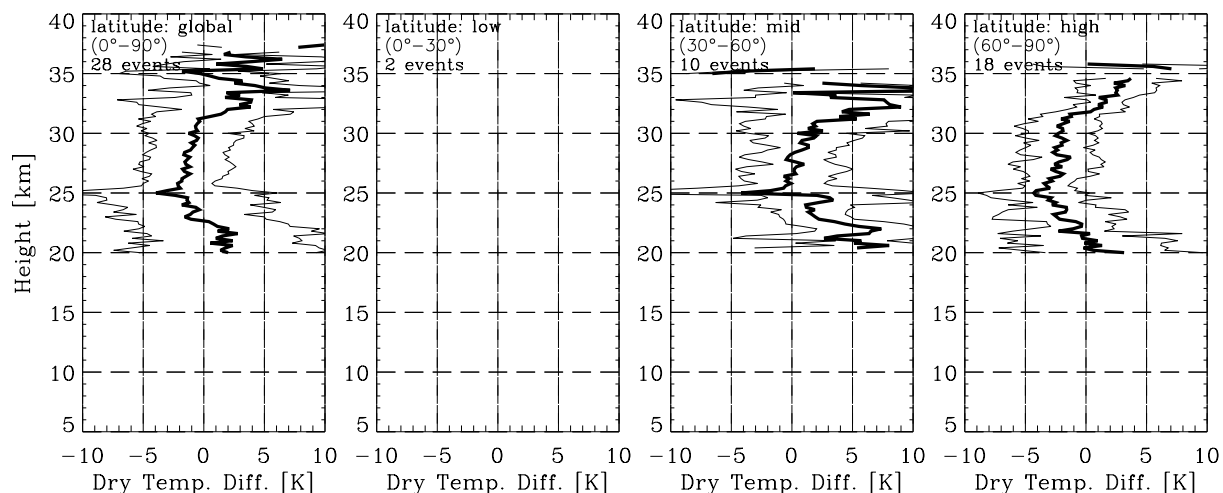


Figure 4.16: Bias \mathbf{b} (bold) and bias \pm standard deviation profiles $\mathbf{b} \pm \mathbf{s}$ (light) of dry temperature retrieved from CHAMP level 2 data with the IGAM/ECMWF scheme relative to coinciding GOMOS/HRTP temperature profiles. Coincidence-criteria: 300 km / 3 hrs. Left panel: global ensemble (28 events), middle-left panel: low-latitude ensemble (2 events, no error statistics possible), middle-right panel: mid-latitude ensemble (10 events), right panel: high-latitude ensemble (18 events). The discrepancy in the sample sizes is due to the fact that in some GOMOS-profiles only few data-points are available. The number of available profiles is defined as the maximum number of data points at all altitude levels which can be smaller than the sum of the profiles.

In the global error statistics, a remarkable, but statistically not significant bias can be found starting from ~ 2 K at 20 km, crossing 0 K at 23 km, negatively peaking with -2 K at 25 km, becoming negative again at 31 km and rising up to ~ 3 K at ~ 33 km. Above that, the bias shows a big variability ranging from -2 K to 7 K. The standard deviation is in the order of 7 K between 20 and 25 km and 3–4 K between 25 and 32 km. The sample sizes of the latitudinal separated ensembles are too small to be interpreted separately.

Interpretation

The available set of profiles for comparison comprises 32 events (see Sect. 3.1.4), only 28 of them contain data-points on common altitude levels, which makes this study statistically not well-founded. In addition, the GOMOS/HRTP data are preliminary, implying that these results have to be interpreted carefully. More than that, they can not be used for validating CHAMP RO measurements yet, the contrary is the case since RO data are much better validated.

This allows some conclusions about the GOMOS/HRTP retrieval: The method basically works and provides atmospheric temperature profiles agreeing with CHAMP-, MIPAS-, and ECMWF-data in the altitude-interval between 20 and ~ 32 km in the range of 5 K. However, many missing data points, and insufficient quality control makes it difficult to use and validate GOMOS/HRTP data. Advancements in this area (reduction of missing data points, quality control), in the reduction of biases, and in the extension of the usable altitude-range are of greatest interest for further HRTP-retrieval algorithm development.

4.3.4 GOMOS/IGAM

Temperature Comparison

Fig. 4.17 shows \mathbf{b} and $\mathbf{b} \pm \mathbf{s}$ profiles of dry temperature retrieved with the IGAM/ECMWF scheme, with respect to GOMOS/IGAM temperature profiles (see Sect. 3.1.4). Due to lacking quality of GOMOS data below 20 km, only the height interval from 20 – 40 km is shown. In the global error statistics, a remarkable and statistically significant cold bias (CHAMP colder than GOMOS) can be found starting from -8 K at 20 km and declining to -3 K at 40 km. The standard deviation amounts to some 8 K between 20 and 25 km, 3 – 6 K between 25 and 35 km, and drastically increasing above that. The sample sizes of the latitudinal separated ensembles are too small to be interpreted separately.

Interpretation

The comparison of preliminary GOMOS/IGAM temperature profiles features a systematical bias (GOMOS/IGAM too warm) of some 5 K. This bias might be due to inconsistencies in the retrieval scheme and promises potential to improve the method. After the reason for the bias is found, the method will deliver valuable temperature observations, especially in the 25 – 35 km altitude interval as indicated by the standard deviation of 3 – 6 K.

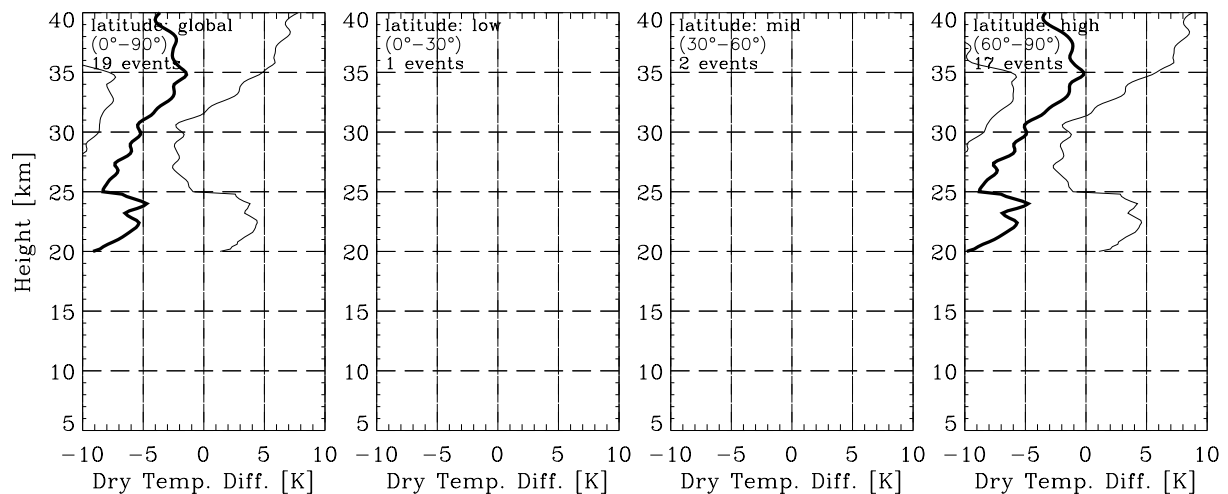


Figure 4.17: Bias \mathbf{b} (bold) and bias \pm standard deviation profiles $\mathbf{b} \pm \mathbf{s}$ (light) of dry temperature retrieved from CHAMP level 2 data with the IGAM/ECMWF scheme relative to coinciding GOMOS/IGAM temperature profiles. Coincidence-criteria: 300 km / 3 hrs. Left panel: global ensemble (19 events), middle-left panel: low-latitude ensemble (1 event, no error statistics possible), middle-right panel: mid-latitude ensemble (2 events, no error statistics possible), right panel: high-latitude ensemble (18 events). The discrepancy in the sample sizes is due to the fact that in some GOMOS-profiles only few data-points are available. The number of available profiles is defined as the maximum number of data points at all altitude levels which can be smaller than the sum of the profiles.

5 Conclusions and Outlook

This report on CHAMPCLIM work package 2 “Radio Occultation Data and Algorithms Validation Based on CHAMP/GPS Data” presented the validation of the advanced geometric optics radio occultation retrieval schemes developed at IGAM/UniGraz applied to data from the CHAMP mission. Such a validation exercise is an indispensable prerequisite for the further application of the algorithms to create RO based global climatologies of refractivity, geopotential height, temperature, and humidity from CHAMP data on a large scale as planned in part 2 of the CHAMPCLIM project. A further aim of this validation study was to find, and allow to subsequently remove, remaining weaknesses in the algorithms.

Within CHAMPCLIM, two retrieval schemes are used at IGAM: The IGAM/MSIS scheme that is independent from model data and uses a search-library of representative atmospheric states for statistical optimization of the retrieval at high altitudes, and the IGAM/ECMWF scheme that uses ECMWF analysis fields for the same purpose. Results from both schemes were validated against a variety of data sources: Against a modeled atmosphere in an end-to-end simulation study, the GFZ operational RO retrieval scheme, numerical weather prediction analyses from ECMWF, and remote-sensing instruments onboard ENVISAT (MIPAS and GOMOS).

The simulation study (Sects. 3.1.1 and 4.1) showed that the newly developed algorithm for obtaining unbiased background information and for fusing it with the observed data (IGAM/MSIS) is principally capable to effectively improve the retrieval performance at high altitudes (above 25 km). However, the background bias correction algorithm involved is not fully effective when applied to CHAMP data (Sect. 4.3) The degraded performance can be explained by residual ionospheric noise stemming from small-scale structures in the ionosphere that were not modeled in the simulation study, by artificial, intermittent error sources in the CHAMP data (e.g., artifacts caused by clock malfunctions), and by the overall noise level of CHAMP data.

However, since RO retrievals independent from NWP analyses are highly desirable, especially for their use in combination with models by means of data assimilation techniques, this scheme will be further developed to become more robust against noisy data, and better profile-search libraries than the MSISE-90 climatology are envisaged. Additionally, it could be demonstrated that refractivity profiles retrieved with IGAM/MSIS as they will be used by a three-dimensional data assimilation (3DVAR) scheme in combination with ECMWF analyses in the second part of CHAMPCLIM are of sufficient quality right now (bias in order of 0.1% up to 35 km, standard deviation below 1% at 5 – 20 km, and ~1.2% up to 32 km). They have the same quality as other retrieval schemes from leading institutions in the field of RO retrieval (Sect. 4.2 and 4.3; Steiner, 2004).

The IGAM/ECMWF retrieval scheme demonstrates that, by careful use of background information, relative independency from the background can be maintained up to at least 40 km whilst the retrieval performance, especially for temperature profiles, is drastically improved. Compared to ECMWF analyses, the IGAM/ECMWF temperature profiles are virtually unbiased between 5 and 30 km and warm biased by ~1.5 K between 30 and 40 km

(demonstrating the relative independence from ECMWF). The comparison to coinciding temperature profiles from ENVISAT/MIPAS (an instrument virtually independent from ECMWF background data) showed a very good agreement in this altitude region, and indicates that the encountered bias is probably attributable to the ECMWF data.

Furthermore, the results of the comparison with ECMWF analyses show that, additionally to the well known negative refractivity bias in the lower troposphere (e.g., Ao et al., 2003), a minor, height-independent constant negative refractivity bias of about -0.4% exists in the RO retrieval results compared to ECMWF analyses. A similar bias compared to ECMWF analyses, at least up to 25 km, can be found in the RO-derived refractivities of other leading institutions (Steiner, 2004; Wickert et al., 2004a; Beyerle et al., 2004), but it was not as clearly identified yet since it is masked by the major refractivity bias in the lower troposphere and by increasing noise and the influence of background information above 25 km. The IGAM/ECMWF retrieval identifies this bias quite clearly as being height-constant, which will help to eliminate it in future algorithm improvements.

Generally, the validation studies presented in this report show that the IGAM RO retrieval schemes are in-line, and in some aspects even better performing, than state-of-the-art retrieval schemes of other institutions. Minor problems encountered during this validation will be subject of further investigation. The IGAM retrieval schemes are prepared for their assignment to produce global RO climatologies based on data from CHAMP, later supplemented by data from future missions such as GRACE, MetOp/GRAS (Silvestrin et al., 2000), COSMIC (Rocken et al., 2000), and ACE+ (Kirchengast and Hoeg, 2004).

Acknowledgments

The authors gratefully acknowledge the GFZ Potsdam, Germany, for the provision of the CHAMP level 2 and level 3 correlative data, for technical support, especially provided by T. Schmidt, and for scientific discussion and advice by J. Wickert. MIPAS temperature profiles were provided by IMK, Univ. of Karlsruhe, Germany. We especially acknowledge the support and discussions concerning the CHAMP-MIPAS validation with D.-Y. Wang from IMK. GOMOS fast photometer temperature profiles were provided by A. Hauchecorne, Service d'Aéronomie du CNRS, Verrières-le-Buisson, France. A. Gobiet and C. Retscher received financial support for the work from the CHAMPCLIM project funded by the Austrian Ministry for Traffic, Innovation, and Technology and managed under Contract No. ASAP-CO-004/03 of the Austrian Space Agency (ASA). Furthermore, A.K. Steiner, U. Foelsche, and A. Gobiet received financial support from the START research award of G.K. funded by the Austrian Ministry for Education, Science, and Culture and managed under Program No. Y103-N03 of the Austrian Science Fund (FWF).

References

- Anthes, R.A.**, C. Rocken, and Y. Kuo, Applications of COSMIC to Meteorology and Climate, *Terrestrial, Atmospheric and Oceanic Sciences*, 11(1), 115-156, 2000.
- Ao, C.O.**, T.K. Meehan, G.A. Hajj, A.J. Mannucci, and G.Beyerle, Lower-Troposphere Refractivity Bias in GPS Occultation Retrievals, *J. Geophys. Res.*, 108 (D18), 4577, 10.1029/2002JD003216, 2003.
- Bevis, M.**, S. Businger, T.A. Herring, C. Rocken, R.A. Anthes, and R.H. Ware, GPS Meteorology: Mapping Zenith Wet Delays onto Precipitable Water, *J. Appl. Met.*, 33, 379-386, 1994.
- Beyerle, G.**, J. Wickert, T. Schmidt, and C. Reigber, Atmospheric sounding by GNSS radio occultation: An analysis of the negative refractivity bias using CHAMP observations, *J. Geophys. Res.*, doi: 10.1029/2003JD003922, 2003.
- Fjeldbo, G.F.**, V.R. Eshleman, and A.J. Kliore, The Neutral Atmosphere of Venus as Studied with the Mariner V Radio Occultation Experiments, *Astron. J.*, 76, 123-140, 1971.
- Foelsche, U.**, and G. Kirchengast, Sensitivity of GNSS radio occultation profiles to horizontal variability in the troposphere: A simulation study, *Proc. 1st Intl. Workshop on Occultations for Probing Atmosphere and Climate*, Sep. 2002, Graz, Austria, Springer Verlag, in press, 2004.
- Foelsche, U.**, G. Kirchengast, and A.K. Steiner, Global climate monitoring based on CHAMP/GPS radio occultation data. *Proc. 1st CHAMP Science Meeting*, Springer-Verlag, Heidelberg, 397-407, 2003.
- Gobiet, A.** and Kirchengast, G., Advancement of GNSS Radio Occultation Retrieval in the Upper Stratosphere, *Proc. 1st Intl. Workshop on Occultations for Probing Atmosphere and Climate*, Sept. 2002, Graz, Austria, Springer Verlag, in press, 2004.
- Gobiet, A.**, G. Kirchengast, J. Wickert, C. Retscher, D.-Y. Wang, and A. Hauchecorne, Evaluation of Stratospheric Radio Occultation Retrieval Using Data from CHAMP, MIPAS, GOMOS, and ECMWF Analysis Fields, *Proc. 2. CHAMP Science Meeting*, Sept. 2003, Potsdam, Springer Verlag, in press, 2004.
- Gorbunov, M.E.**, Canonical transform method for processing radio occultation data in the lower troposphere, *Radio Sci.*, 37(5), 1057, doi:10.1029/2000RS002592, 2002.
- Hajj, G.A.**, C.O. Ao, B.A. Iijima, D. Kuang, E.R. Kursinski, A.J. Mannucci, T.K. Meehan, L.J. Romans, M. de la Torre Juarez, and T.P. Yunck, CHAMP and SAC-C Atmospheric Occultation Results and Intercomparisons, *J. Geophys. Res.*, submitted, 2003.
- Hedin, A.E.**, Extension of the MSIS thermosphere model into the middle and lower atmosphere, *J. Geophys. Res.*, 96, 1159-1172, 1991.
- Hocke, K.**, Inversion of GPS meteorology data. *Annales Geophysicae* 15: 443–450, 1997.
- Hocke, K.**, A.G. Pavelyev, O.I. Yakovlev, L. Barthes, and N. Jakowski, Radio occultation data analysis by the radiographic method, *J. Atmos. Terr. Phys.*, 61, 1169–1177, 1999.
- Hocke, K.**, K. Igarashi, and T. Tsuda, High-resolution profiling of layered structures in the lower stratosphere by GPS occultation, *Geophys. Res. Lett.*, 30(8), 1426, doi:10.1029/2002GL016566, 2003.
- IPCC**, Climate Change 2001 – The Scientific Basis. Contribution of WG I to the 3rd Assessment Report of the IPCC, edited by D.L. Albritton et al., Cambridge University Press, Cambridge, 2001.
- Jensen, A.S.**, M.S. Lohmann, H-H. Benzon, and A.S. Nielsen, Full spectrum inversion of radio occultation signals, *Radio Sci.*, 38(3), 1040, doi:10.1029/2002RS002763, 2003.

RO Data and Algorithms Validation Based on CHAMP/GPS Data

CHAMPCLIM – Radio Occultation Data Analysis and Climate Monitoring based on CHAMP/GPS

- Kirchengast, G.**, P. Hoeg, The ACE+ mission: an Atmosphere and Climate Explorer based on GPS, GALILEO, and LEO-LEO radio occultation, *Proc. 1st Intl. Workshop on Occultations for Probing Atmosphere and Climate*, Sept. 2002, Graz, Austria, Springer Verlag, in press, 2004.
- Kirchengast, G.**, J. Fritzer, and J. Ramsauer, End-to-end GNSS Occultation Performance Simulator Version 4 (EGOPS4) Software User Manual (Overview and Reference Manual), *Techn. Report for ESA/ESTEC*, Inst. for Geophys., Astrophys., and Meteorol., Univ. of Graz, Austria, No. 5/2001.
- Kirchengast, G.**, A.K. Steiner, U. Foelsche, L. Kornblueh, E. Manzini, and L. Bengtsson, Spaceborne Climate Change Monitoring by GNSS Occultation Sensors, *Proc. 11th Symp. on Global Change Studies*, Amer. Met. Soc. Annual Meeting 2000, Long Beach/CA, U.S.A., 62-65, 2000.
- Kursinski, E.R.**, G.A. Hajj, W.I. Bertiger, S.S. Leroy, T.K. Meehan, L.J. Romans, J.T. Schofield, D.J. McCleese, W.G. Melbourne, C.L. Thornton, T.P. Yunck, J.R. Eyre, and R.N. Nagatani, Initial Results of Radio Occultation of Earth's Atmosphere Using the Global Positioning System. *Science*, 271, 1107-1110, 1996.
- Kursinski, E.R.**, G.A. Hajj, J.T. Schofield, R.P. Linfield, and K.R. Hardy, Observing Earth's Atmosphere with Radio Occultation Measurements Using the Global Positioning System, *J. Geophys. Res.*, 102, 23429-23465, 1997.
- Leitinger, R.**, and G. Kirchengast, Easy to Use Global and Regional Models – a Report on Approaches Used in Graz, *Acta Geod. Geophy. Hung.*, 32, 329-342, 1997.
- Randel, W.**, M.L. Chanin, C. Michaut, SPARC intercomparison of middle atmosphere climatologies. *SPARC Report No. 3*, WCRP 116, WMO/TD 11424, 2002.
- Retscher, C.**, A. Gobiet, and G. Kirchengast, Stratospheric temperature and ozone sounding with ENVISAT/GOMOS stellar occultation, *Proc. 1st Int'l Workshop on Occultations for Probing Atmosphere and Climate (OPAC-1)*, Sept. 2002, Graz, Austria, Springer Verlag, in press, 2004.
- Rocken, C.**, Y. Kuo, W.S. Schreiner, D. Hunt, S. Sokolovskij, C. McCormick, COSMIC System Description. *Terr., Atmos. and Oceanic Sci.* 11: 21–52, 2000.
- Rocken, C.**, R. Anthes, M. Exner, D. Hunt, S. Sokolovskiy, R. Ware, M. Gorbunov, W. Schreiner, D. Feng, B. Herman, Y.H. Kuo, and X. Zou, Analysis and Validation of GPS/MET Data in the Neutral Atmosphere, *J. Geophys. Res.*, 102(D25), 29849-29866, 1997.
- Roeckner, E.**, L. Bengtson, J. Feichter, J. Lelieveld, and H. Rodhe, Transient climate change simulations with a coupled atmosphere-ocean GCM including the tropospheric sulfur cycle. *J. Climate*, 12, 10, pp 3004 – 3032, 1999.
- Silvestrin P.**, R. Bagge, M. Bonnedal, A. Carlström, J. Christensen, M. Hägg, T. Lindgren, and F. Zangerl, Spaceborne GNSS radio occultation instrumentation for operational applications, *Proc 13th ION-GPS Meeting 2000*, Salt Lake City, UT, USA, 2002.
- Sokolovskiy, S.V.**, Effect of superrefraction on inversions of radio occultation signals in the lower troposphere, *Radio Sci.*, 38(3), 1058, doi:10.1029/2002RS002728, 2003.
- Sokolovskiy, S.**, and D. Hunt, Statistical Optimization Approach for GPS/Met Data Inversions, paper presented at URSI GPS/Met Workshop, Tucson, Arizona, 1996.
- Steiner, A.K.**, Error Analyses of Refractivity Profiles Retrieved from CHAMP Radio Occultation Data, *Danish Meteorological Institute (DMI) Scientific Report*, 04-02, Copenhagen, Denmark, 2004.
- Steiner, A.K.**, G. Kirchengast, U. Foelsche, L. Kornblueh, E. Manzini, and L. Bengtsson, GNSS Occultation Sounding for Climate Monitoring, *Phys. Chem. Earth A*, 26, 13-124, 2001.
- Steiner, A.K.**, G. Kirchengast, and H.P. Ladreiter, Inversion, Error Analysis and Validation of GPS/MET Occultation Data, *Ann. Geophys.*, 17, 22-138, 1999.

- Syndergaard, S.**, D. Flittner, R. Kursinski, D. Feng, B. Herman, and D. Ward, Simulating the influence of horizontal gradients on retrieved profiles from ATOMS occultation measurements – a promising approach for data assimilation, *Proc. 1st Intl. Workshop on Occultations for Probing Atmosphere and Climate*, Sept. 2002, Graz, Austria, Springer Verlag, in press, 2004.
- von Clarmann, T.**, N. Glatthor, U. Grabowski, M. Höpfner, S. Kellmann, M. Kiefer, A. Linden, G. Mengistu Tsidu, M. Milz, T. Steck, G. P. Stiller, D. Y. Wang, H. Fischer, B. Funke, S. Gil-López, and M. López-Puertas, Retrieval of temperature and tangent altitude pointing from limb emission spectra recorded from space by the Michelson Interferometer for Passive Atmospheric Sounding (MIPAS), *J. Geophys. Res.*, 108, D23, 4736, doi:10.1029/2003JD003602, 2003a.
- von Clarmann, T.**, S. Ceccherini, A. Doicu, A. Dudhia, B. Funke, U. Grabowski, S. Hilgers, V. Jay, A. Linden, M. López-Puertas, F.-J. Martín-Torres, V. Payne, J. Reburn, M. Ridolfi, F. Schreier, G. Schwarz, R. Siddans, and T. Steck, A blind test retrieval experiment for infrared limb emission spectrometry, *J. Geophys. Res.*, 108, D23, 4746, doi:10.1029/2003JD003835, 2003b.
- Vorob'ev, V.V.** and T.G. Krasnil'nikova, Estimation of the Accuracy of the Atmospheric Refractive Index Recovery from Doppler Shift Measurements at Frequencies Used in the NAVSTAR System, *Phys. Atmos. Ocean*, 29, 602-609, 1994.
- Wang, D.Y.**, J. Wickert, G. Stiller, T. Clarmann, G. Beyerle, T. Schmidt, M.L. Puertas, B. Funke, S. Gil-López, N. Glatthor, U. Grabowski, M. Höpfner, S. Kellmann, M. Kiefer, A. Linden, G.M. Tsidu, M. Milz, T. Steck, H. Fischer, and Ch. Reigber, Comparisons of MIPAS/ENVISAT and GPS-RO/CHAMP Temperature Profiles, *Proc. 2. CHAMP Science Meeting*, Sept. 2003, Potsdam, Springer Series, in press, 2004
- Ware, R.**, M. Exner, D. Feng, M. Gorbunov, K. Hardy, B. Herman, Y. Kuo, T. Meehan, W. Melbourne, C. Rocken, W. Schreiner, S. Sokolovskiy, F. Solheim, X. Zou, R. Anthes, S. Businger, and K. Trenberth, GPS Sounding of the Atmosphere from Low Earth Orbit: Preliminary Results, *Bull. Amer. Met. Soc.*, 77, 19-40, 1996.
- Wickert, J.**, A. Gobiet, G. Beyerle, A. Steiner, G. Kirchengast, U. Foelsche, T. Schmidt, GPS radio occultation with CHAMP: Comparison of atmospheric profiles from GFZ Potsdam and IGAM Graz, *Proc. 2nd CHAMP Science Meeting*, Sept. 2003, Potsdam, Germany, Springer Verlag, in press, 2004a.
- Wickert, J.**, T. Schmidt, G. Beyerle, G. Michalak, R. König, J. Kaschenz, and C. Reigber, Atmospheric profiling with CHAMP: Status of the operational data analysis, validation of the recent data products and future prospects, *Proc. 2nd CHAMP Science Meeting*, Sept. 2003, Potsdam, Germany, Springer Verlag, in press, 2004b.

(intentionally left blank, back page if double-sided print)

Appendix A: CHAMP – ECMWF Error Statistics, Compiled

In Appendix A we present a comprehensive compilation of the validation of all CHAMP-temperature profiles (retrieved with the IGAM-retrieval schemes) used in this report with respect to co-located temperature profiles derived from operational ECMWF analyses (see Sect. 3.1.3). The results are presented as error statistic profiles showing the bias **b** (bold line) and the bias \pm standard deviation **b** \pm **s** profiles (light lines). These quantities were calculated based on IGAM – ECMWF differences and are shown for both IGAM retrieval schemes, IGAM/MSIS and IGAM/ECMWF (see Sect. 2).

IGAM – GFZ Retrieval Intercomparison Ensemble

January 1 – 7, 2003

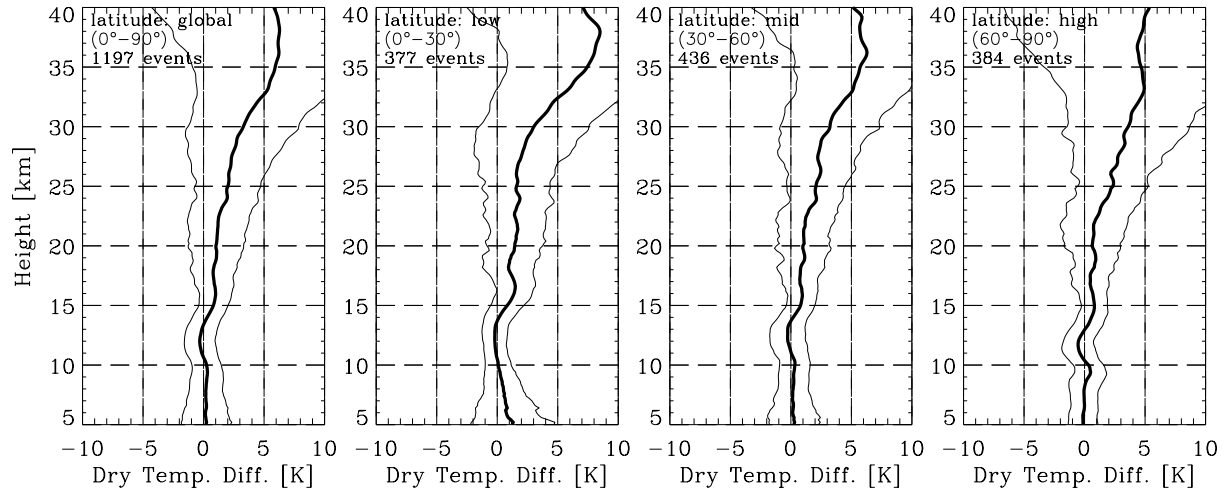


Figure A.1: Bias b (bold) and bias \pm standard deviation profiles $b \pm s$ (light) of dry temperature retrieved from CHAMP level 2 data with the IGAM/MSIS scheme relative to temperatures derived from co-located ECMWF operational analyses. Left panel: global ensemble (1197 occultation events), middle-left panel: low-latitude ensemble (377 events), middle-right panel: mid-latitude ensemble (436 events), right panel: high-latitude ensemble (384 events).

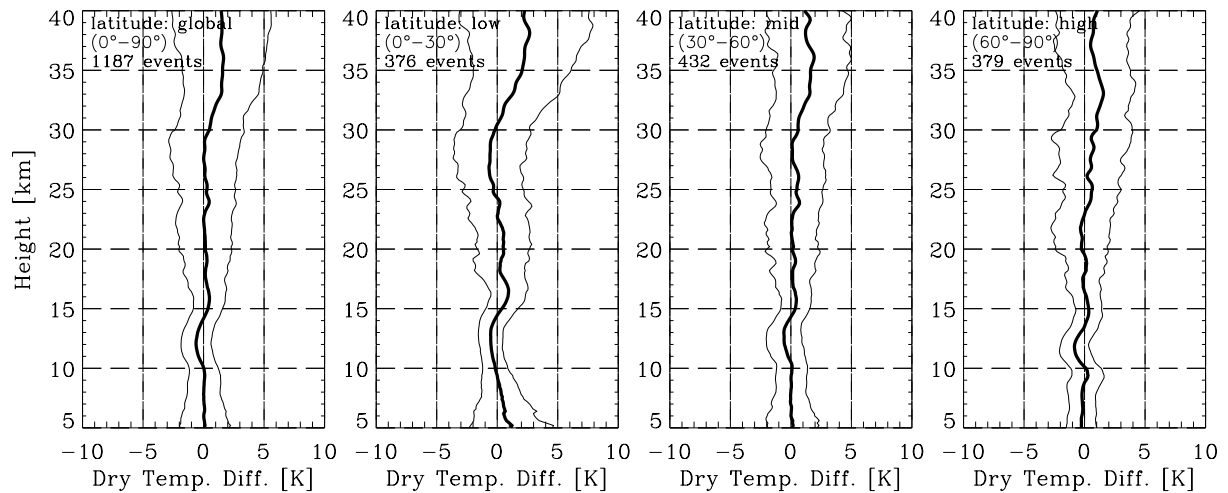


Figure A.2: Bias b (bold) and bias \pm standard deviation profiles $b \pm s$ (light) of dry temperature retrieved from CHAMP level 2 data with the IGAM/ECMWF scheme relative to temperatures derived from co-located ECMWF operational analyses. Left panel: global ensemble (1187 occultation events), middle-left panel: low-latitude ensemble (376 events), middle-right panel: mid-latitude ensemble (432 events), right panel: high-latitude ensemble (379 events).

ENVISAT/MIPAS Validation Ensemble

September 8, 12, 14 – 28, 2002

October 11 – 13, 2002

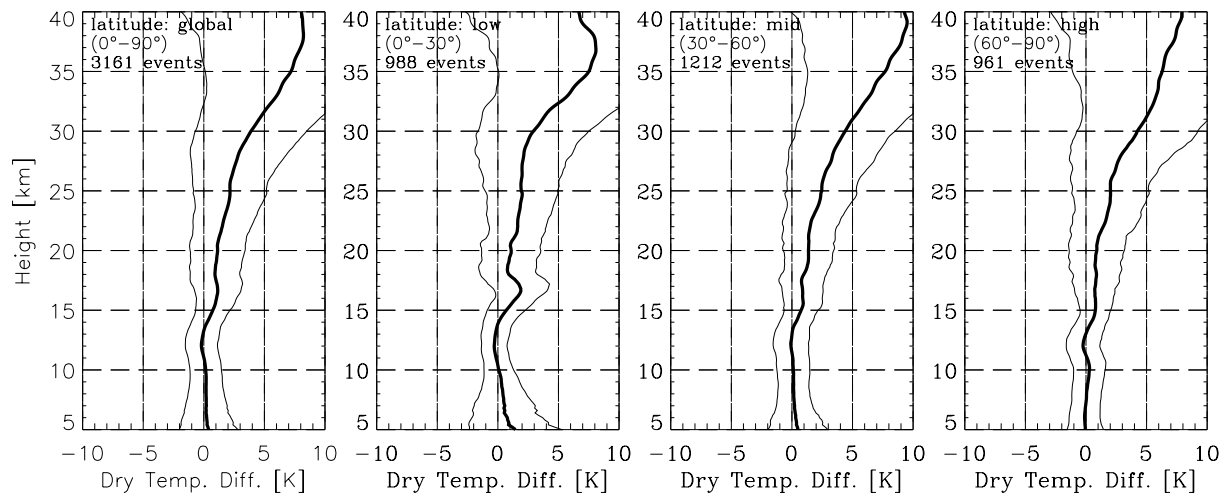


Figure A.3: Bias b (bold) and bias \pm standard deviation profiles $b \pm s$ (light) of dry temperature retrieved from CHAMP level 2 data with the IGAM/MSIS scheme relative to temperatures derived from co-located ECMWF operational analyses. Left panel: global ensemble (3161 occultation events), middle-left panel: low-latitude ensemble (988 events), middle-right panel: mid-latitude ensemble (1212 events), right panel: high-latitude ensemble (961 events).

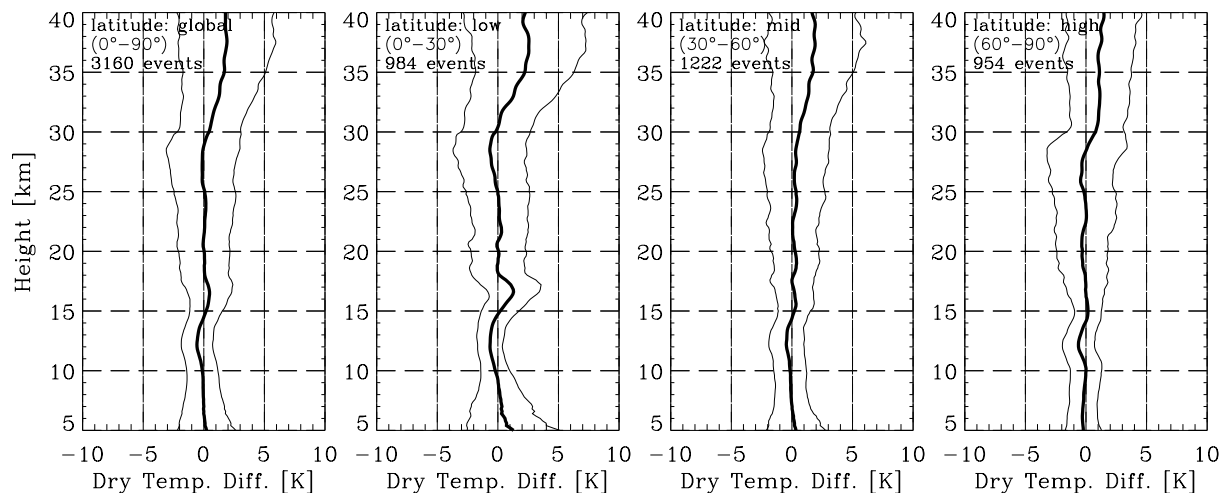


Figure A.4: Bias b (bold) and bias \pm standard deviation profiles $b \pm s$ (light) of dry temperature retrieved from CHAMP level 2 data with the IGAM/ECMWF scheme relative to temperatures derived from co-located ECMWF operational analyses. Left panel: global ensemble (3160 occultation events), middle-left panel: low-latitude ensemble (984 events), middle-right panel: mid-latitude ensemble (1222 events), right panel: high-latitude ensemble (954 events).

ENVISAT/GOMOS Validation Ensemble

September 20 – 27, 2002

October 11 – 13, 2002

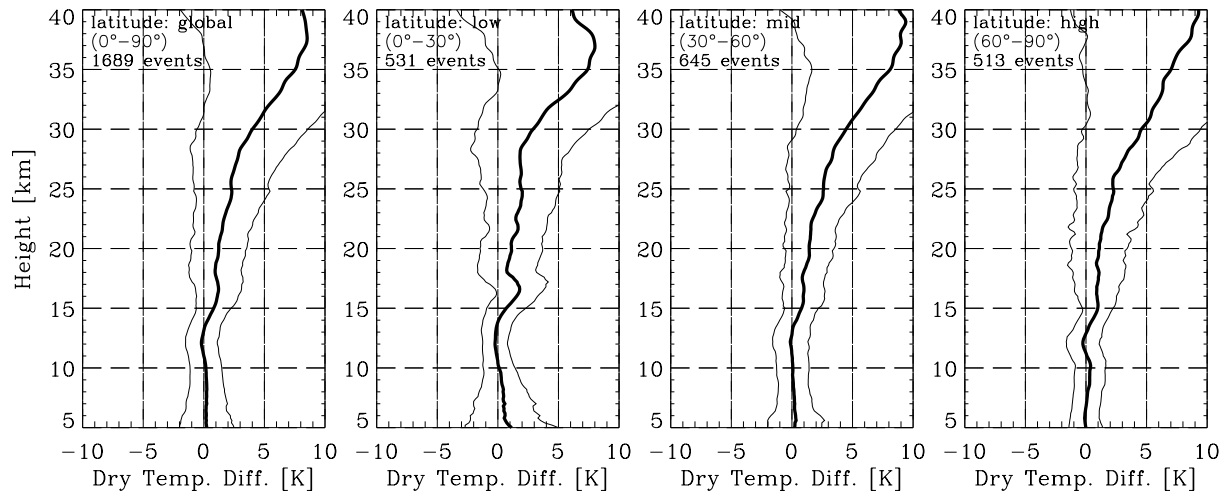


Figure A.5: Bias b (bold) and bias \pm standard deviation profiles $b \pm s$ (light) of dry temperature retrieved from CHAMP level 2 data with the IGAM/MSIS scheme relative to temperatures derived from co-located ECMWF operational analyses. Left panel: global ensemble (1689 occultation events), middle-left panel: low-latitude ensemble (531 events), middle-right panel: mid-latitude ensemble (645 events), right panel: high-latitude ensemble (513 events).

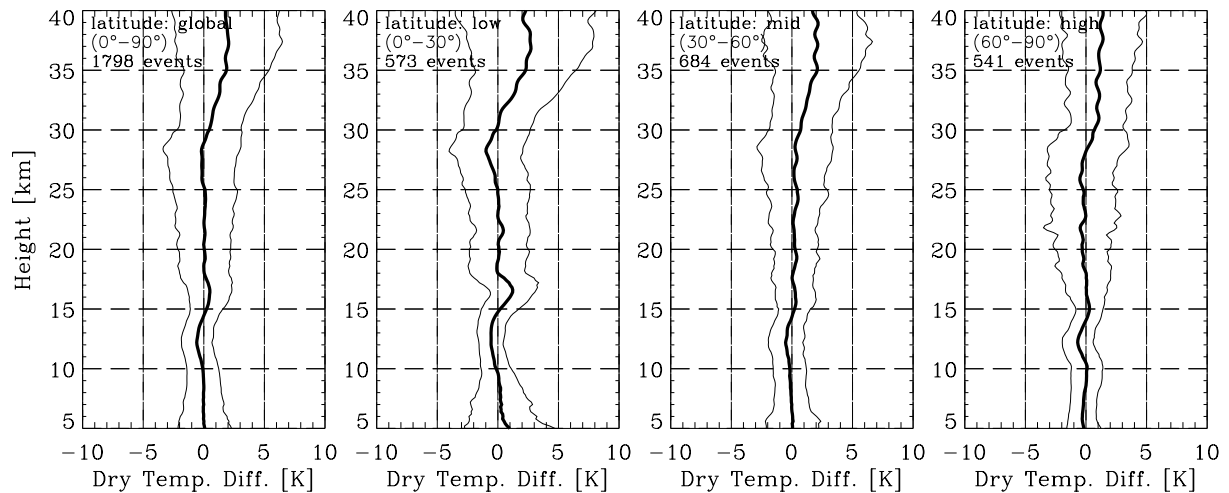


Figure A.6: Bias b (bold) and bias \pm standard deviation profiles $b \pm s$ (light) of dry temperature retrieved from CHAMP level 2 data with the IGAM/ECMWF scheme relative to temperatures derived from co-located ECMWF operational analyses. Left panel: global ensemble (1798 occultation events), middle-left panel: low-latitude ensemble (573 events), middle-right panel: mid-latitude ensemble (684 events), right panel: high-latitude ensemble (541 events).

Appendix B: CHAMP – ECMWF Tropopause Temperature Differences, Examples

In Appendix B we exemplarily present selected CHAMP-RO temperature profiles (retrieved with the IGAM/ECMWF scheme) compared to co-located ECMWF analysis temperatures focusing on the tropopause-region (see also Sect. 4.3.1). Each plot depicts temperature profiles derived from CHAMP RO data (black line) and from ECMWF operational analyses (gray line) in the left panel and the difference $T_{\text{CHAMP}} - T_{\text{ECMWF}}$ in the right panel. Dates identifying the locations and times of the occultation events are given in the figure captions.

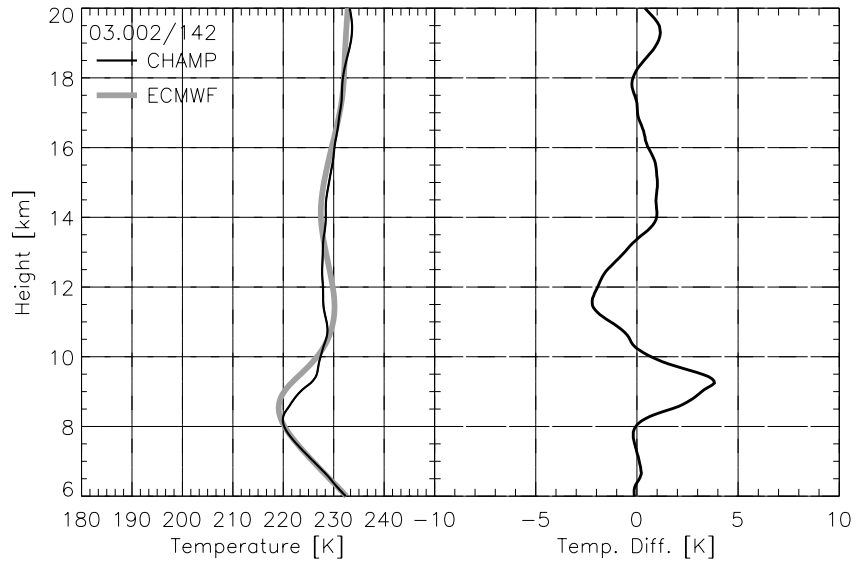


Figure B.1: Temperature profile derived from CHAMP (-76.3° latitude, 116.2° longitude, Jan 2, 2003, 12:10 UT, IGAM/ECMWF retrieval) compared to collocated temperatures from ECMWF operational analyses. Left panel: temperature profiles. Right panels: Difference $T_{\text{CHAMP}} - T_{\text{ECMWF}}$.

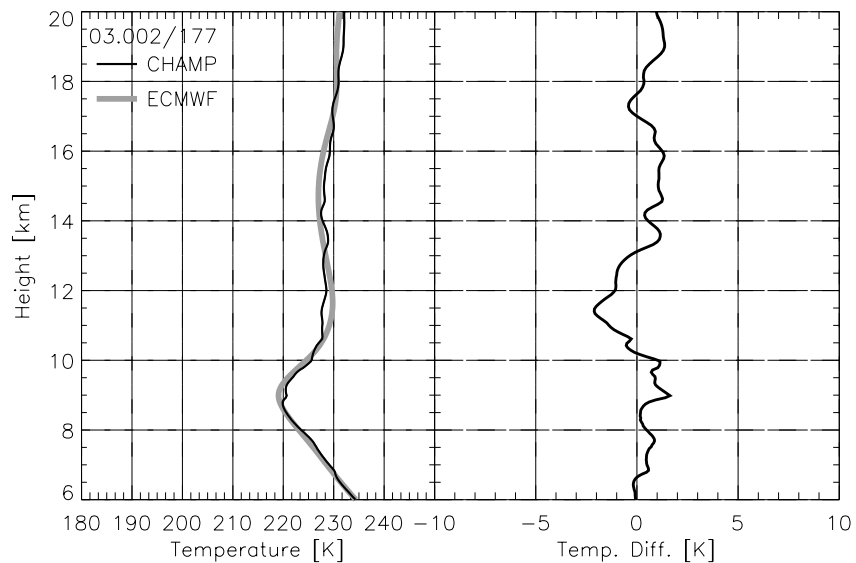


Figure B.2: Temperature profile derived from CHAMP (-75.2° latitude, 133.2° longitude, Jan 2, 2003, 15:19 UT, IGAM/ECMWF retrieval) compared to collocated temperatures from ECMWF operational analyses. Left panel: temperature profiles. Right panels: Difference $T_{\text{CHAMP}} - T_{\text{ECMWF}}$.

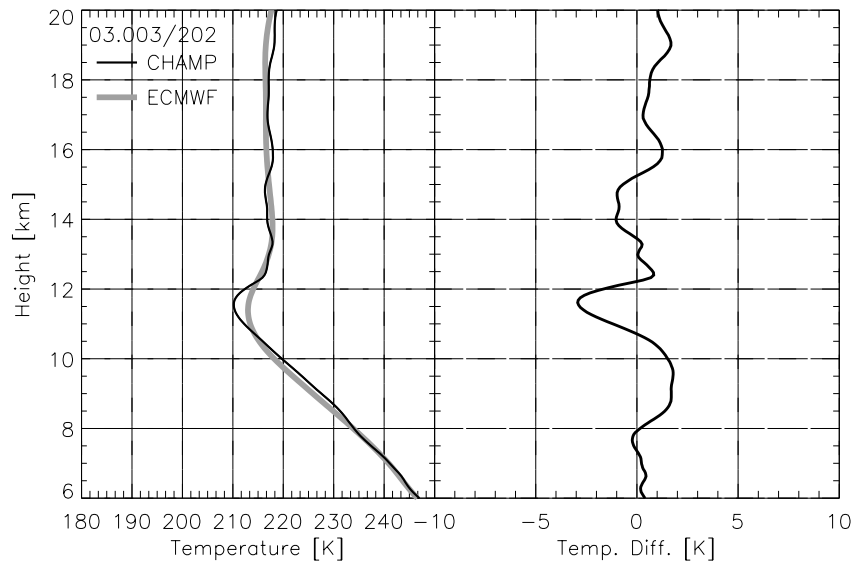


Figure B.3: Temperature profile derived from CHAMP (-44.2° latitude, -40.5° longitude, Jan 3, 2003, 18:56 UT, IGAM/ECMWF retrieval) compared to collocated temperatures from ECMWF operational analyses. Left panel: temperature profiles. Right panels: Difference $T_{\text{CHAMP}} - T_{\text{ECMWF}}$.

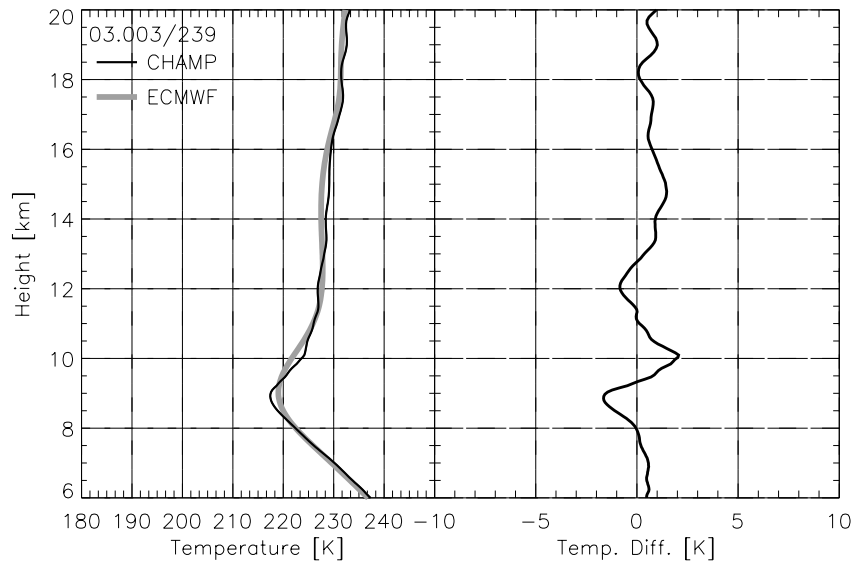


Figure B.4: Temperature profile derived from CHAMP (-73.9° latitude, -38.3° longitude, Jan 3, 2003, 22:10 UT, IGAM/ECMWF retrieval) compared to collocated temperatures from ECMWF operational analyses. Left panel: temperature profiles. Right panels: Difference $T_{\text{CHAMP}} - T_{\text{ECMWF}}$.

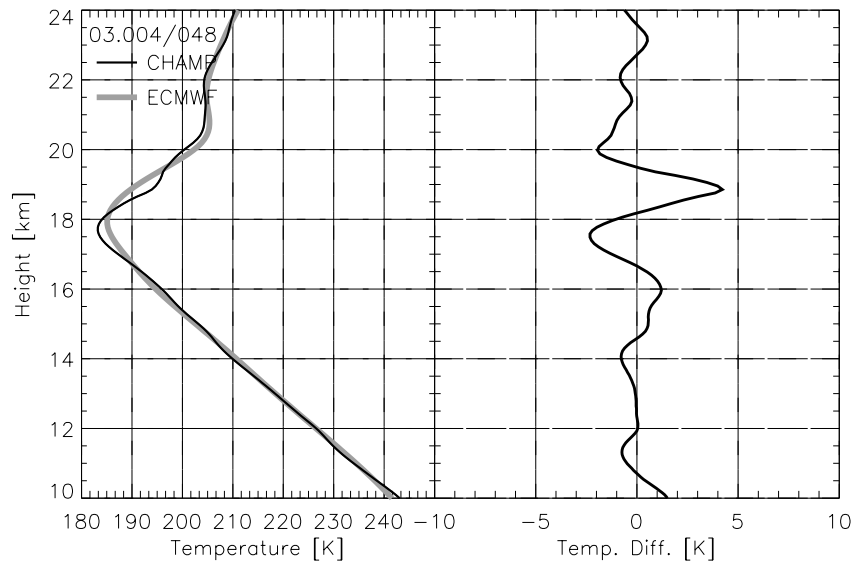


Figure B.5: Temperature profile derived from CHAMP (-7.1° latitude, -161.8° longitude, Jan 4, 2003, 04:01 UT, IGAM/ECMWF retrieval) compared to colocated temperatures from ECMWF operational analyses. Left panel: temperature profiles. Right panels: Difference $T_{\text{CHAMP}} - T_{\text{ECMWF}}$.

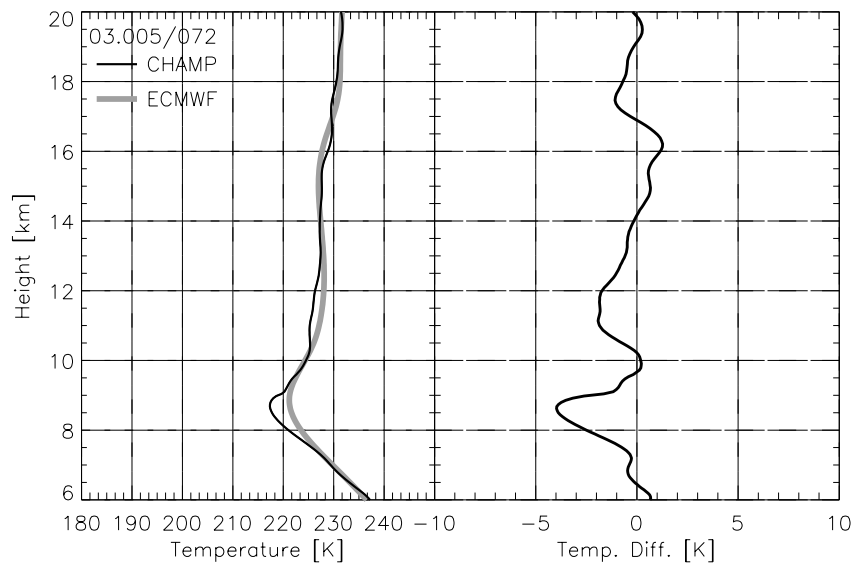


Figure B.6: Temperature profile derived from CHAMP (-76.1° latitude, -53.4° longitude, Jan 5, 2003, 06:44 UT, IGAM/ECMWF retrieval) compared to colocated temperatures from ECMWF operational analyses. Left panel: temperature profiles. Right panels: Difference $T_{\text{CHAMP}} - T_{\text{ECMWF}}$.

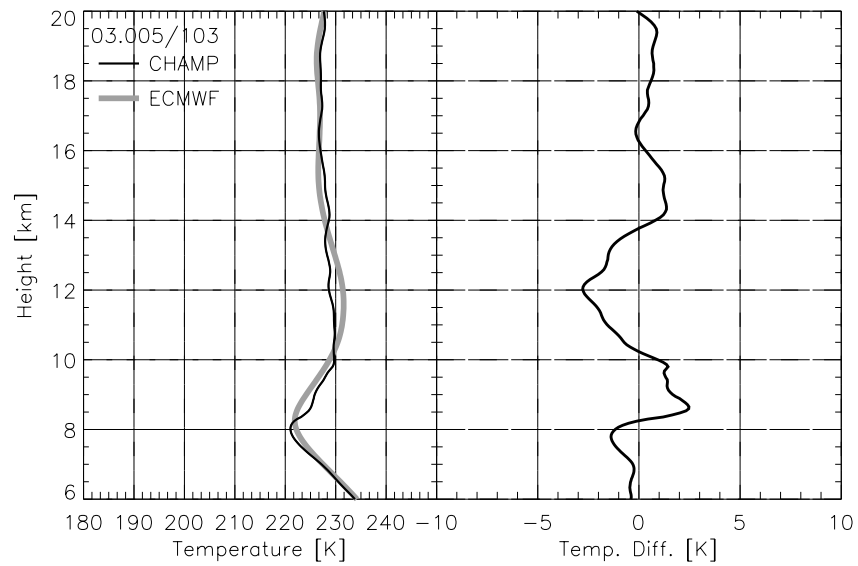


Figure B.7: Temperature profile derived from CHAMP (-56.6° latitude, 91.3° longitude, Jan 5, 2003, 09:37 UT, IGAM/ECMWF retrieval) compared to collocated temperatures from ECMWF operational analyses. Left panel: temperature profiles. Right panels: Difference $T_{\text{CHAMP}} - T_{\text{ECMWF}}$.

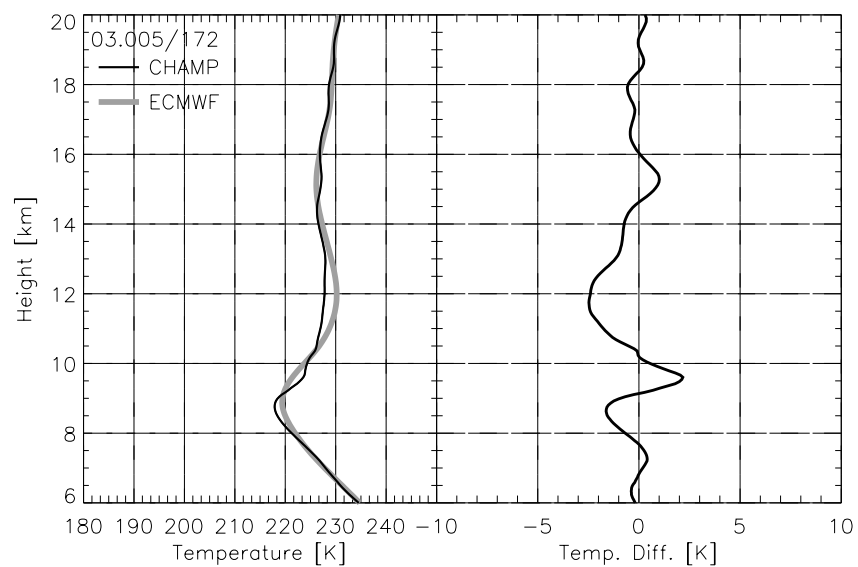


Figure B.8: Temperature profile derived from CHAMP (-65.0° latitude, 41.0° longitude, Jan 5, 2003, 15:51 UT, IGAM/ECMWF retrieval) compared to collocated temperatures from ECMWF operational analyses. Left panel: temperature profiles. Right panels: Difference $T_{\text{CHAMP}} - T_{\text{ECMWF}}$.

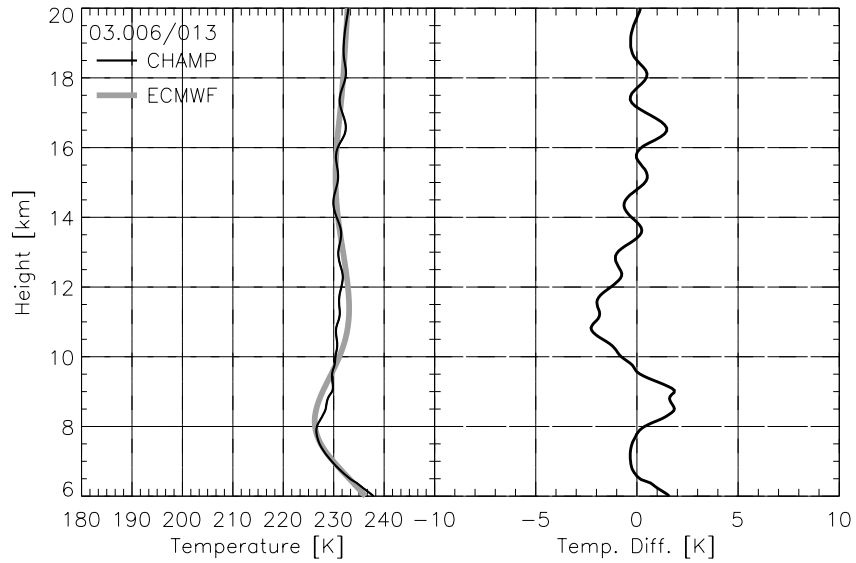


Figure B.9: Temperature profile derived from CHAMP (-69.2° latitude, -110.8° longitude, Jan 6, 2003, 01:09 UT, IGAM/ECMWF retrieval) compared to colocated temperatures from ECMWF operational analyses. Left panel: temperature profiles. Right panels: Difference $T_{\text{CHAMP}} - T_{\text{ECMWF}}$.

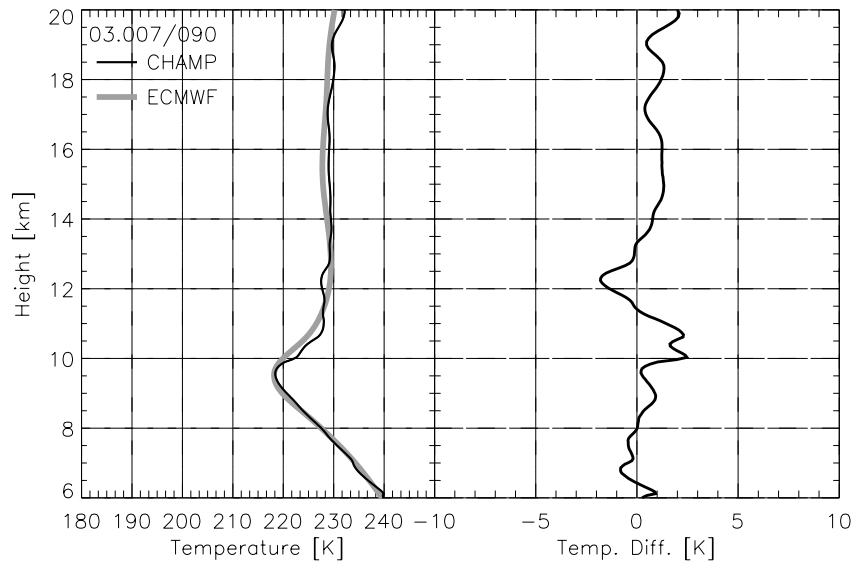


Figure B.10: Temperature profile derived from CHAMP (-67.1° latitude, 156.7° longitude, Jan 7, 2003, 08:03 UT, IGAM/ECMWF retrieval) compared to colocated temperatures from ECMWF operational analyses. Left panel: temperature profiles. Right panels: Difference $T_{\text{CHAMP}} - T_{\text{ECMWF}}$.

Ω end of document Ω